NAVIGATION BY WEAVER ANTS IN AN UNFAMILIAR, FEATURELESS ENVIRONMENT

Theerawee   Thiwatwaranikul

A Thesis Submitted in Partial Fulfillment of the Requirements for the

Degree of Master of Science in Physics

Suranaree University of Technology

Academic Year 2019

การเดินทางของมดแดงภายใต้สภาพแวดล้อมที่
ไม่คุ้นเคยและไร้ลักษณะพิเศษเฉพาะ

นายธีรวีร์ ธิวัฒน์วรานิกุล

วิทยานิพนธ์นี้เป็นส่วนหนึ่งของการศึกษาตามหลักสูตรปริญญาวิทยาศาสตรมหาบัณฑิต
สาขาวิชาฟิสิกส์
มหาวิทยาลัยเทคโนโลยีสุรนารี
ปีการศึกษา 2562

NAVIGATION BY WEAVER ANTS IN AN

UNFAMILIAR, FEATURELESS ENVIRONMENT

Suranaree University of Technology has approved this thesis submitted in partial fulfillment of the requirements for a Master's Degree.

Thesis Examining Committee

_____

(Assoc. Prof. Dr. Puangratana Pairor)

Chairperson

_____
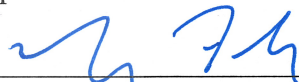
(Asst. Prof. Dr. Michael F. Smith)

Member (Thesis Advisor)

_____

(Dr. Sukrit Suksombat)

Member

_____

(Dr. Wittawat Saenrang)

Member
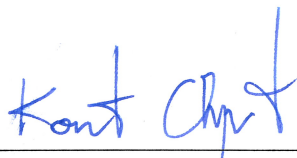
_____
(Assoc. Prof. Flt. Lt. Dr. Kontorn Chamniprasart)

Vice Rector for Academic Affairs

and Internationalization

_____
(Assoc. Prof. Dr. Worawat Meevasana)

Dean of Institute of Science

ธีรวีร์ ธิวัฒน์วรานิกุล : การเดินทางของมดแดงภายใต้สภาพแวดล้อมที่ไม่คุ้นเคยและไร้ลักษณะพิเศษเฉพาะ (NAVIGATION BY WEAVER ANTS IN AN UNFAMILIAR, FEATURELESS ENVIROMENT). อาจารย์ที่ปรึกษา : ผู้ช่วยศาสตราจารย์ ดร.ไมเคิล เอฟ สมิธ, 64 หน้า

มดแดง/ ทฤษฏีแลงกวิน/ การเคลื่อนที่แบบบราวน์

การเคลื่อนที่ของมดแดงสายพันธุ์ *Oecophylla smaragdina* ในบริเวณที่สะอาดหรือบริเวณที่ถูกเคลือบด้วยสารเคมีไล่แมลง ถูกติดตามด้วยระบบวิดีทัศน์และคอมพิวเตอร์ เราพัฒนาแบบจำลองเชิงทฤษฎีซึ่งสอดคล้องกับทฤษฎีแลงกวินเพื่ออธิบายการเคลื่อนที่แบบบราวน์ของมดแดง แบบจำลองดังกล่าวประกอบด้วยแรงขับแบบสุ่มที่เปลี่ยนแปลงความเร็วของมดในแต่ละช่วงขณะเวลา และแรงที่เกี่ยวข้องกับขอบของพื้นที่และสารเคมีไล่แมลงซึ่งมีผลต่อการเปลี่ยนแปลงความเร็วของมด ฟังก์ชันการแจกแจงความน่าจะเป็นของแรงขับแบบสุ่มมีรูปแบบที่ชัดเจนและเรียบง่ายในเชิงคณิตศาสตร์ อีกทั้งมดยังมีการตอบสนองต่อสารไล่แมลงในลักษณะเดียวกันกับอนุภาคตอบสนองต่อกำแพงศักย์โดยมดจะเคลื่อนที่ช้าลงก่อนกลับสู่สภาวะสมดุลของการเคลื่อนที่แบบบราวน์ การเคลื่อนที่ของมดโดยเฉลี่ยแล้วสามารถอธิบายได้ด้วยแบบจำลองที่ให้ข้อมูลเชิงลึกที่มดใช้สำหรับการเดินทาง

สาขาวิชาฟิสิกส์   ลายมือชื่อนักศึกษา_____
ปีการศึกษา 2562   ลายมือชื่ออาจารย์ที่ปรึกษา_____

THEERAWEE THIWATWARANIKUL : NAVIGATION BY WEAVER
ANTS IN AN UNFAMILIAR, FEATURELESS ENVIRONMENT,
THESIS ADVISOR : ASST. PROF. MICHAEL F. SMITH, Ph.D. 64 PP.

WEAVER ANTS/ LANGEVIN THEORY/ BROWNIAN MOTION

The motion of individual weaver ants, members of the species *Oecophylla smaragdina*, was tracked in time as they moved in a small, clean arena and one partly covered by a chemical repellent. We develop a theoretical model, analogous to the Langevin theory of Brownian motion. The model includes random local impulses that change ant velocity with each time step and deterministic forces, associated with the arena boundaries and repellent, that gradually change ant velocity. The probability distribution function of random impulses is robust and mathematically simple and ants respond to the repellent, much as a particle responds to a potential energy barrier, by initially slowing before recovering towards the equilibrium state of Brownian motion. The motion of the average individual can be characterized by the model, which provides some insight into the algorithm the ant employs for navigation.

School of Physics	Student's Signature _____
Academic Year 2019	Advisor's Signature _____

ACKNOWLEDGEMENTS

Theerawee Thiwatwaranikul

CONTENTS

CONTENTS (Continued)

CONTENTS (Continued)

LIST OF TABLES

LIST OF TABLES (Continued)

LIST OF FIGURES

LIST OF FIGURES (Continued)

LIST OF FIGURES (Continued)

LIST OF FIGURES (Continued)

LIST OF FIGURES (Continued)

LIST OF FIGURES (Continued)

LIST OF ABBREVIATIONS

RGB   Reg-Green-Blue

PDF   Probability distribution function

CHAPTER I

INTRODUCTION

1.1 Background

This chapter includes a brief review of some previous work on ant behavior, mainly related to large-scale organization and navigation. We also present the goals of our research and introduce the tools and techniques that we have used to try to accomplish these goals.

1.1.1 Large-scale organization of weaver ants

"Intelligence is the ability to adapt to change."

– Stephen Hawking

Oecophylla smaragdina, a species commonly known as weaver ants, are native to Asia and Africa. Weaver ants perform large-scale cooperative efforts (Hölldobler and Wilson, 1990; Hölldobler and Wilson, 1994) that are impressive, even compared to those of other ant species. As anyone living in Thailand can attest, thousands of weaver ant individuals work together to weave nests in trees, by folding and gluing broad leaves. They also form bridges from their own bodies. Whenever individuals work together successfully, communication is required. For such large projects, constructed by many ants working in different places at the same time, communication has to occur on long length scales (Mlot et al., 2011; Sakiyama, 2017; Vernerey et al., 2018).

      The mechanisms of communication that weaver ants use include

pheromones, gestures and direct contact. They are complex and sophisticated. For decades, biologists have been interested in the mechanisms and effects of weaver ant communication (Cole Jr and Jones Jr, 1948; Hölldobler, 1983; Kamhi et al., 2015; Golden and Hill, 2016). For physicists like us, they make weaver ants interesting for their demonstration of collective phenomena in complex systems (Czirók et al., 1999; Vicsek et al., 1999; Vicsek and Zafeiris, 2012; DeLellis et al., 2014).

Biological systems, particularly groups of animals, provide many other examples of complex interacting systems. While different species have their own specific features, some universal properties are expected. This is analogous to the universality predicted by statistical physics for condensed matter systems, especially near a phase transition (Landau and Lifshitz, 1980; Pathria and Beale, 1996; Tong, 2012).

Two different condensed matter systems will have very different microscopic physics but, near a phase transition, behave similarly. When water changes to ice, molecules that are far apart participate together in this transition. Since the motion of distant molecules is correlated, one doesn't have to follow the microscopic details to understand this transition. This is what makes it possible for two systems, with different microscopic details, to have similar long-distance correlations during their respective phase transitions.

So it is not too surprising that the motion of fish schools, flocking birds, swarms of insects and other systems display very similar large scale patterns. All these groups of animals produce collective motion ranging from orderly through turbulent to random (Becco et al., 2006). Similar mathematical approaches, even the same governing equations, can be used to describe all of them. When we observe the motion of weaver ants, we are hoping to use these ants as a laboratory for studying more general properties of complex systems.
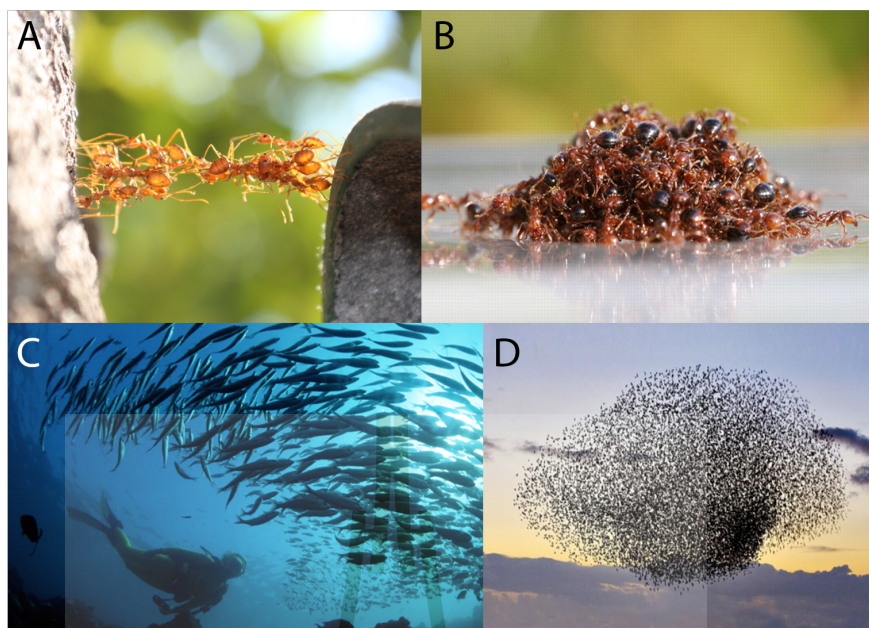
Figure 1.1 A gallery of images related to the collective behavior and large-scale organization in different species. **(A)** Living bridge by the Asian weaver ants *Oecophylla smaragdina.* Groups of workers arrange themselves into multiple chains of their own bodies and pull together to close the gap. The figure was obtained from the website, https://en.wikipedia.org/wiki/Ant. **(B)** The aggregation of fire ants, *Solenopsis invicta.* Ants can considerably enhance their water repellency by linking their bodies together. They build a living raft. The figure was retrieved from (Mlot et al., 2011). **(C)** Shoaling behavior in fish derive many benefits including defense against predators (by diluting the chance of capture), enhanced foraging success and higher success in finding a mate. **(D)** Thousands of starlings produce a fascinating aerial display. They are also trying to avoid a predator bird close to the central. The figure was retrieved from (Pokhrel and Kayastha, 2018).

1.1.2 Navigation and Brownian motion of ants

Weaver ants modify their foraging motion in response to communications in obvious ways (Hölldobler and Wilson, 1978; Franks and Richardson, 2006; Gordon,

2010; Golden and Hill, 2016). One individual will recruit others for foraging missions, or two partners will move together in tandem runs. The long-term goal of our work is to look for more subtle effects of communication. Can we detect, by analyzing the statistics of ant motion, how one ant modifies its navigation algorithm in response to information passed from another? We are hoping to determine how ants organize their motion in response to communication taking place between them.

Before we can reach this long-term goal, we must complete a crucial first step: understanding the navigation algorithm of a single ant in the absence of communicated information. We have to establish a baseline navigation algorithm for the individual ant. Once we know how a single ant navigates, we can look for modifications it makes in response to communication from its fellows.

So, while communication between ants and the resulting behavior of the complex system is the motivation for our work, this report will not touch on ant-to-ant communication directly. Here, we study individual ants, who have no one to communicate with. It is meant as the preliminary stage of a larger project. Surprisingly, the subject of the navigation of an individual ant turns out to be interesting in its own right. There is enough here, in the motion of a weaver ant individual, to provide for a decent thesis.

There is an apparent similarity between the erratic motion of a foraging ant and Brownian motion. A Brownian motion picture is often taken as a basis for more elaborate theories of navigation by ants and many other animals (Vicsek et al., 1995; Schweitzer et al., 1998; Viswanathan et al., 1999; West and Nonnenmacher, 2001; Wehner, 2003; Kohler and Wehner, 2005; Sims et al., 2008; Reynolds and Rhodes, 2009; Humphries et al., 2010; Bazazi et al., 2012; Bialek, 2012; Romanczuk et al., 2012; Reynolds, 2012; Sims et al., 2012; Raichlen et al.,

2014; Schultheiss et al., 2015; Gire et al., 2016). Much current research along these lines is motivated by the idea of using ant motion as an example of general collective motion of communicating individuals: as macroscopic versions of bacterial processes relevant to medicine, as models for human crowds or for designs of swarming robots (Krieger et al., 2000; Kube and Bonabeau, 2000; Deisboeck and Couzin, 2009; Esponda and Gordon, 2015; Chung and Lin, 2017).

A Brownian particle, like a grain of pollen in water, undergoes dispersive motion because of its collisions with surrounding water molecules. Einstein explained the motion using a statistical description of these collisions, and Langevin further developed this theory a few year later (Pathria and Beale, 1996). In Langevin's theory of Brownian motion, the particle is subject to random impulses, forces applied over a short duration, that have random direction and zero time average, as well as deterministic forces like the average drag force and interaction with external fields.

Below we will develop a version of Langevin theory and apply it to ant motion in a non-descript arena. Since the dominant forces on the ant are reaction forces of the ground on its moving body parts, the parameters in the Langevin theory can be interpreted as values that the ant chooses to use for its purpose of navigating within the arena. So, if we are able to explain ant movement with a Langevin model then we will have a picture of the ant individual's navigation algorithm.

1.1.3 Images of an ecosystem

The history of animal behavior science has been dominated by qualitative studies: scientists observe animals in laboratories or in nature and try to understand their complex motivations and strategies as they perform various tasks (Tinbergen,

1963; Altmann, 1974). In this thesis, we are studying a very simple aspect of animal behavior, the motion of single ant, which affords us the opportunity to take a more quantitative approach.

A major theme of this work is our effort to avoid, whenever possible, any subjective characterization of ant behavior and any speculation about the intention of the ant. We do not define, as many researchers do, different qualitative phases of animal behavior–such as pausing, resting, grooming or whatever (Camargo et al., 2017; Palavalli-Nettimi and Narendra, 2018). We think defining ant motion in this way would introduce our own subjective judgement to the analysis and, since we are new to this field, are wary of doing it. Similarly, we are not going to guess why an ant decides to move as it does. Instead, we will gather strictly *quantitative* information about the ant motion and then try to analyze this data.

The data will be obtained via image-based tracking techniques. Such techniques are now in common usage in studies of fish and birds, particularly (Dankert et al., 2009; Ballerini et al., 2008; Lukeman et al., 2010; Audira et al., 2018) or school fish (Audira et al., 2018). These studies use three-dimensional reconstruction technique to obtain the spatial positions of an individual within a group. The tracking technique provides highly precise and accurate behavioral data (Dell et al., 2014). Of course, our project is much less technologically demanding: we are only tracking an individual ant and two-dimensional tracking is sufficient.

Image-based tracking involves three main steps as shown in Figure 1.2, (i) data saved from a video file as image sequences; (ii) detection of the individual position in each image that are linked over multiple frames to form trajectories through time; (iii) analysis of trajectories and other behavioral data. (Strictly speaking, it is the optical center of mass of the 2D-projection of the ant's body.) All of our analysis will be based on the position-time data of each ant individually.
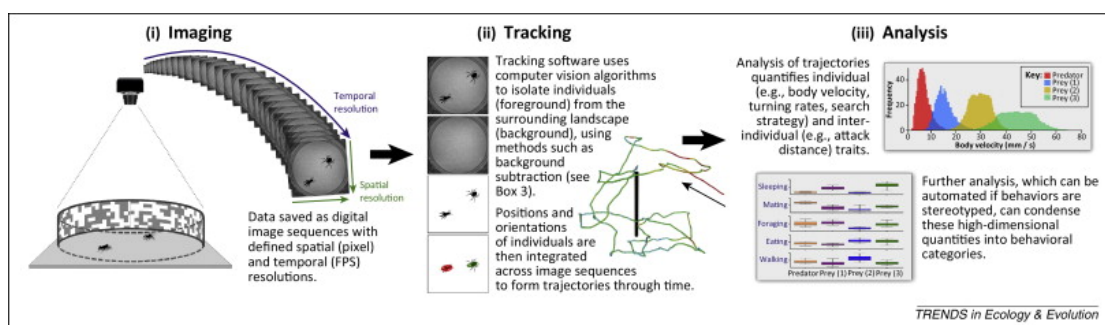
Figure 1.2 The three general steps of image-based tracking of animal behavior are (i) Imaging, obtaining a sequence of images. (ii) Tracking and (iii) analysis of trajectories or other behavioral data. The figure retrieved from (Dell et al., 2014).

1.2 Project summary

In this research, we take a quantitative approach to a simple aspect of the behavior of an individual weaver ant, its motion within a small featureless arena. We track each ant's position versus time. Based on the results, we develop a model of individual ant movement that is analogous to the Langevin theory of Brownian motion. The algorithm, employed by the ant for navigation, is represented by the parameters of this model.

CHAPTER II

METHODOLOGY

2.1   Experimental design

The motion of weaver ant, *Oecophylla smaragdina*, individuals was observed and recorded. Below, we describe the preparation and experimental techniques, including insect collection, video recordings and image processing methods that we used for the experiments.

2.1.1   Ethics statement

Individual ants that were captured in the wild were studied in the laboratory and released at the same location they were found within hours. All efforts were made to minimize suffering of ants.

2.1.2   Insect collection

Individual major-workers from *Oecophylla smaragdina*, belonging to one of several colonies, were captured in the wild from wooded areas. We used a clean plastic box to capture each individual ant and transport it to the laboratory without otherwise touching the ant.

2.1.3   Experimental setup

The motion of ants was studied in two similar configurations. In both cases, the ant was free to move on the surface of a square plate, ceramic floor tile, with a

Figure 2.1 Asian weaver ants, *Oecophylla smaragdina*, from a wild near the laboratory.

side length $L = 30$ cm and a thickness of 0.6 cm. The plate was in a larger tray containing water, not deep enough to reach the plate surface, so individual ant at the plate edges encountered a water barrier that they rarely attempted to cross.

In the first configuration, the plate is clean, so the square arena was approximately homogeneous. In the second, a central rectangular band was coated evenly with 1% w/w citronella oil, a natural repellent that is harmful but non-lethal to ants (Wang et al., 2015; Wang et al., 2016). This band, of width ℓ, is referred to as zone $\mathcal{R}$ in Figure 2.2B. Values, $\ell = 2.5$ and 10 cm, were used in different experiments. We use x, y position coordinates with the origin at the plate center. The arena is defined by $-L/2 \leq x \leq L/2$ and $-L/2 \leq y \leq L/2$ or $|x| \leq 15$ cm, $|y| \leq 15$ cm. The repellent, when present, is coated evenly over the region $|x| < \ell/2$.

For each trial, a single ant, having been captured using a clean plastic container, was transferred into the arena by inverting this container. Within a few minutes of each ant being introduced, we started recording its motion with

a video camera and did so for time $T = 300$ seconds before similarly removing it from the arena. A typical ant continued moving throughout each trial.

The high-speed camera was fixed to a tripod and positioned directly above the arena. In-house image processing scripts coded in MATLAB extracted the position of the ant from the images. (Details about the image processing are included in the next section.) Two-dimensional spatial coordinates $\mathbf{r}(t) = (x(t), y(t))$ were obtained at discrete time steps $t = j\Delta t$ with $j = 0, 1, 2, ..., 4500$ and $\Delta t = 1/15$ s.
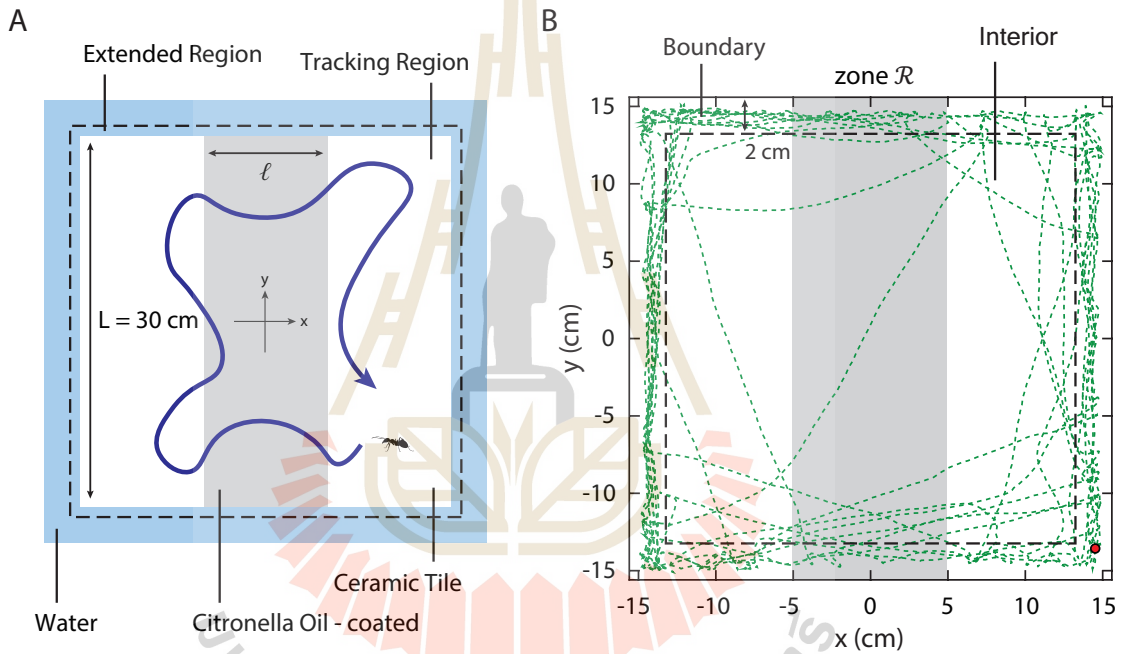
Figure 2.2 (A) An illustration of an experimental setup for observing ant movement with a camera mounted above the arena, a square floor tile of length $L = 30$ cm. The position of an ant can be detected slightly beyond the boundary of the arena, in the extended region about 0.5 cm. **(B)** The green path is an actual single ant trajectory, with one point per time step Δt, in a clean arena. The gray band divides the arena into zones, which have no significance for the clean arena but indicate where (zone $\mathcal{R}$) citronella oil is to be added.

2.2   Image-based tracking method

In the video recording process, we placed the ant gently in the arena and maintained a temperature of 25 ± 2^oC in the laboratory. Each ant underwent a single trial, lasting five minutes. Its motion was recorded using a digital HD video camera (digital sampling rate of thirty frames per second). To process the image, we tracked the ant position using a MATLAB program and image tracking process was done as follows:

1. Import an RGB image of each frame of the video and change the image size by selecting an image that includes the centered square plate and a rim, of width roughly 0.5 cm, of surrounding water (Note that the position of the ant, determined by its optical center of mass, can move slightly outside the arena even if the ant does not walk into the water).

2. Each RGB image is converted to a gray scale and a background image obtained by averaging over all frames.

3. From each RGB image, converted to gray scale, we subtract the background image. This gives us a picture of ant.

4. We adjust the intensity (contrast and saturation) of the resulting image to see the ant more clearly and then convert each gray scale image to a binary image (black-white scale) by intensity threshold.

5. To reduce noise, we remove all points that are significantly bigger or smaller than average ant size.

6. We identify a spatial coordinate $\mathbf{r}(t) = (x(t), y(t))$ at each time step using the mean of the binary function.

Note that, we extract a spatial position of an ant using two consecutive frames. So, the fraction of time $\Delta t = 2/30$ s is the smallest time step we can use. According to the camera's spatial resolution, $x = 30$ cm/1010 pixels $= 0.03$ cm

per pixel, this is the smallest distance we can resolve.
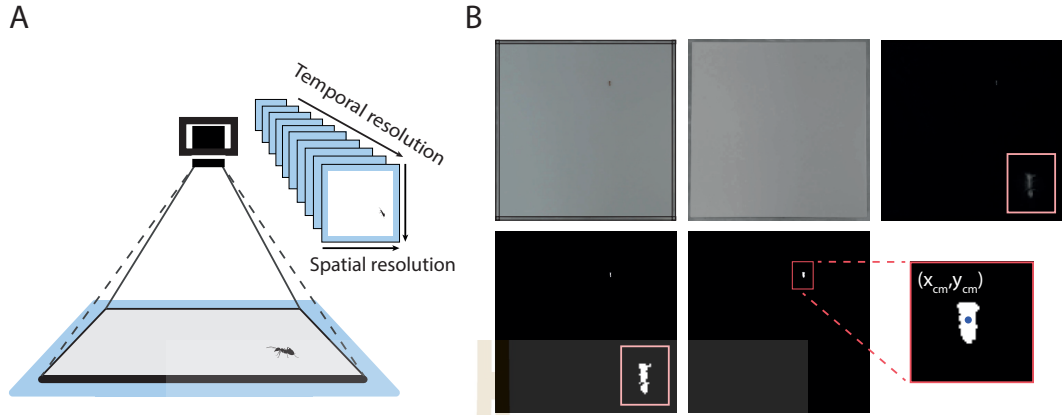
Figure 2.3 The image processing steps used for tracking weaver ant motion. **(A)** An illustration for the experimental setup. Imaging: data saved as a digital image sequences with a certain spatial resolution (limited by square pixel length, Δx) and temporal resolution (limited by frames per second, $1/\Delta t$) over a total duration of $T = 300$ s. **(B)** Tracking: software uses in-house computer vision algorithms for isolate and identify the ant position, then assign it spatial coordinates (the position of the optical center of mass) by subtracting it from of an individual ant from the background image.

2.3 Preliminary results

Sample data showing an ant trajectory is shown in Figure 2.2B. Because of the ant's finite body size, its position is occasionally found in the extended region, about 0.5 cm beyond the arena. Position histograms are shown in Figure 2.4. For these, we amassed data $(x(t), y(t))$ (without distinguishing individuals) and counted the number of events where x, y landed in each square bin $\Delta x = 0.6$ cm in length, at time t. Dividing by the total number of events, this gives a probability density $\Pi(x, y, t)$ for finding an ant near $\mathbf{r} = (x, y)$ at time t. Averaging over

time gives the normalized histogram $\Pi(x, y) = 1/T \int dt \Pi(x, y, t)$ that tells us the fraction of time that the average ant spends near a given position.

From the results, Figure 2.2B and Figure 2.4, ants are often found near the arena boundary. They have a slightly reduced probability to be found within the repellent–the average probability for ants to be in zone $\mathcal{R}$ with and without the repellent is 0.20 ± 0.01 and 0.23 ± 0.01, respectively. The repellent does not have a pronounced effect on probability density overall. This is noteworthy, and may be contrasted with the clear effect of repellent on specific properties of motion discussed in detail below.

To model and analyze ant motion, we exploit the square symmetry of the arena that results in approximate square symmetry for the data in the clean arena. This symmetry is only approximate–the position of the tripod, room lighting, etc., were not arranged carefully to maintain it. Non-zero average deviations from square symmetry can likely be attributed to ants using long-range perception. We observe such a deviation below, but it is a small effect. The raw data consists of the position and time measurements. Other experimental properties, like the time-dependent squared velocity of ensembles of ants and the probability of crossing through zone $\mathcal{R}$ when repellent is present, are discussed in the next section. These are all obtained by re-organizing and analyzing $x(t), y(t)$.
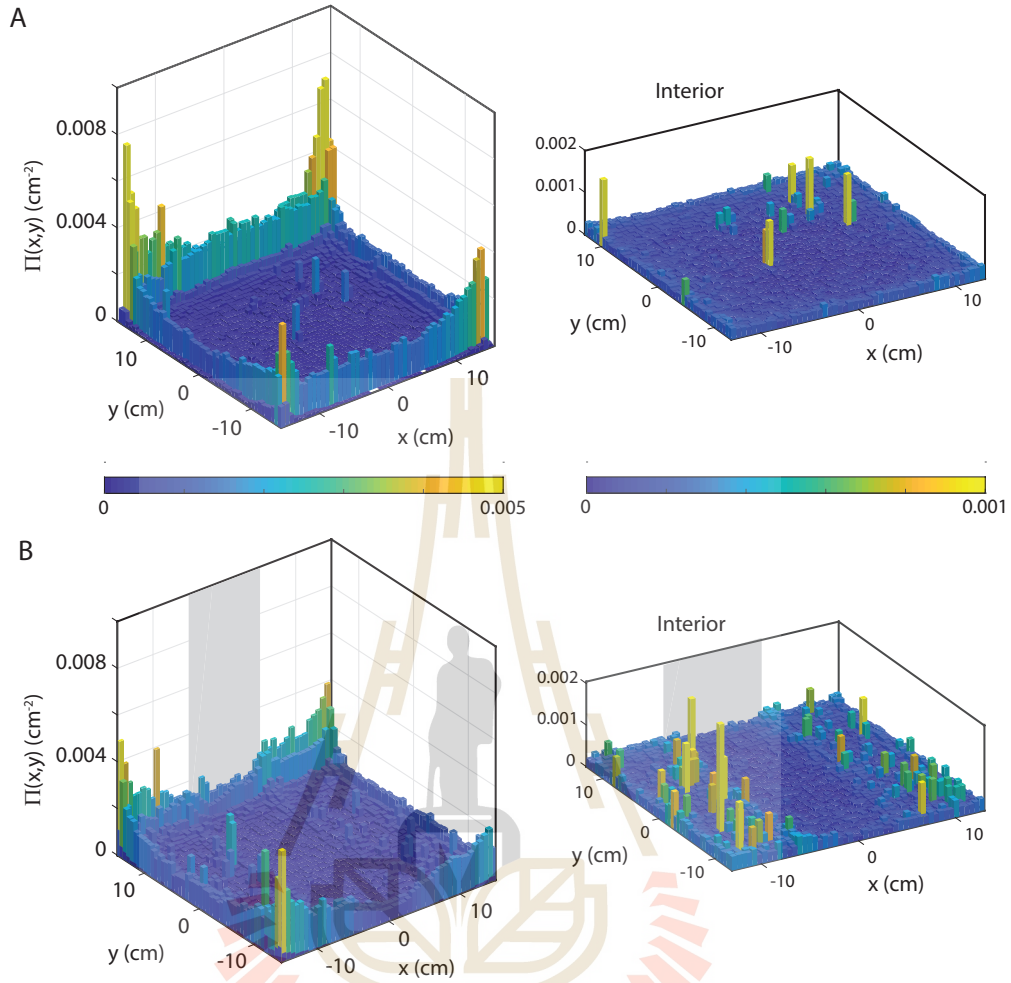
Figure 2.4 Time-averaged position histograms. Left: **(A)** A normalized histogram of ant position for 59 ants in a clean arena, indicating the fraction of time ants spent near a given position (x, y). **(B)** Normalized histogram of ant position for 68 ants with the repellent, citronella oil, painted in zone $\mathcal{R}$ (gray band) when $\ell = 10$ cm. Ants have a strong tendency to remain near the arena boundaries and have a lower probability overall to be found within zone $\mathcal{R}$ when repellent is present (though this effect is not immediately obvious from the histograms shown). Right: The normalized histogram of ant position in the central region or "interior" (defined in Figure 2.2B), for removing the edge dominant. Significantly different in **(A)** homogeneous and **(B)** heterogeneous domains, has a repelling strip.

CHAPTER III

THEORETICAL MODEL OF ANT MOTION

Most statistical properties of the data can be captured by a simple theoretical model in which the ant is treated as particle undergoing Brownian motion. In the first section, we use a broad overview of the data to motivate this model then apply it to make non-trivial predictions of its more specific properties. More detail will be discussed in the model calculation section.

3.1 Velocity and velocity-change distributions

The position $\mathbf{r}_i(t) = (x_i(t), y_i(t))$ of $i = 1, 2, 3, ..., 59$ ant individuals in the clean arena with the time evolution t in steps $\Delta t = 1/15$ s from $t = 0$ to $t = 300$ s was measured. From it, we derive the velocity $\mathbf{v}_i(t) = \Delta \mathbf{r}_i / \Delta t$ with $\Delta \mathbf{r}_i = \mathbf{r}_i(t + \Delta t) - \mathbf{r}_i(t)$ and change in velocity $\Delta \mathbf{v}_i = \mathbf{v}_i(t + \Delta t) - \mathbf{v}_i(t)$ at each time step (except the last two). All points are included in a single full dataset $(i, t, x, y, v_x, v_y, \Delta v_x, \Delta v_y)$. To unclutter notation, the label i of the ant will no longer be written explicitly.

Figures 3.1A, 3.2A present normalized histograms and maps in phase space, respectively. We defined a probability distribution of velocity, $\Pi(v_x, v_y, t)$, the probability of finding an ant with a velocity in a bin centered on v_x, v_y at time t. Averaging this over time yields $\Pi(v_x, v_y) = 1/T \int dt \Pi(v_x, v_y, t)$. To obtain a one-dimensional histogram, we can further integrate $\Pi(v_x, v_y)$ over all v_y. The resulting distribution, giving the average probability of finding an ant with a given v_x, is shown in Figure 3.1A. Curves are shown for both v_x and v_y for the 'Clean' arena and for an arena with the 'Repellent' citronella oil present for $|x| < \ell/2 = 5$ cm.

This distribution is peaked at zero with shoulder features at $v \approx 5 - 6$ cm/s. A typical ant does not remain still for long but, since it passes through zero velocity each time it turns around, has a high probability to have a small velocity. The shoulder features are notably missing from the v_x distribution when citronella oil is present.

Figures 3.2A show maps in (v_x, v_y) space, with one data point per time step per ant. These date were divided according to position: data for the 'Interior' have positions at least $d = 2$ cm away from any boundary, $|x| < L/2 - d, |y| < L/2 - d$, while data for the 'Boundary' were obtained within the boundary strip of width d. The latter looks like a plus sign because ants move along the boundaries.
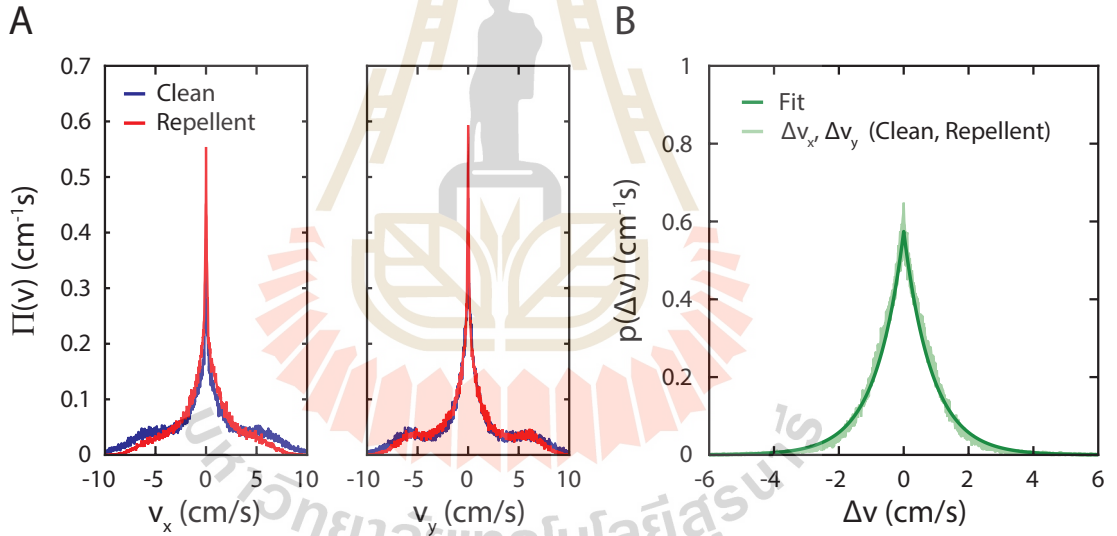
Figure 3.1 Ant velocity and change in velocity derived from the position data of Figure 2.4. **(A)** Normalized histograms of velocity v_x (Left) and v_y (Right) for all ants at all times in a clean arena (blue) and in an arena with repellent present in zone $\mathcal{R}$, $\ell = 10$ cm (red). **(B)** The light green is normalized histogram for velocity changes Δv_x and Δv_y occurring with each time step. The dark-green line is the one-parameter fit to Eq.3.2 with $m = 1$.

We also constructed histograms and phase space maps for the change in

velocity $(\Delta v_x, \Delta v_y)$, shown in Figures 3.1B, 3.2B. The phase space maps are approximately isotropic. The probability distributions for Δv_x and Δv_y are symmetric, peaked at zero, and do not change noticeably when repellent is added. These simple distributions motivate the application of Langevin theory: velocity changes can be attributed to random local impulses with a robust probability distribution. Distributions over velocity and position are more complicated because they result from an accumulation of many successive impulses and are strongly affected by the arena boundaries.
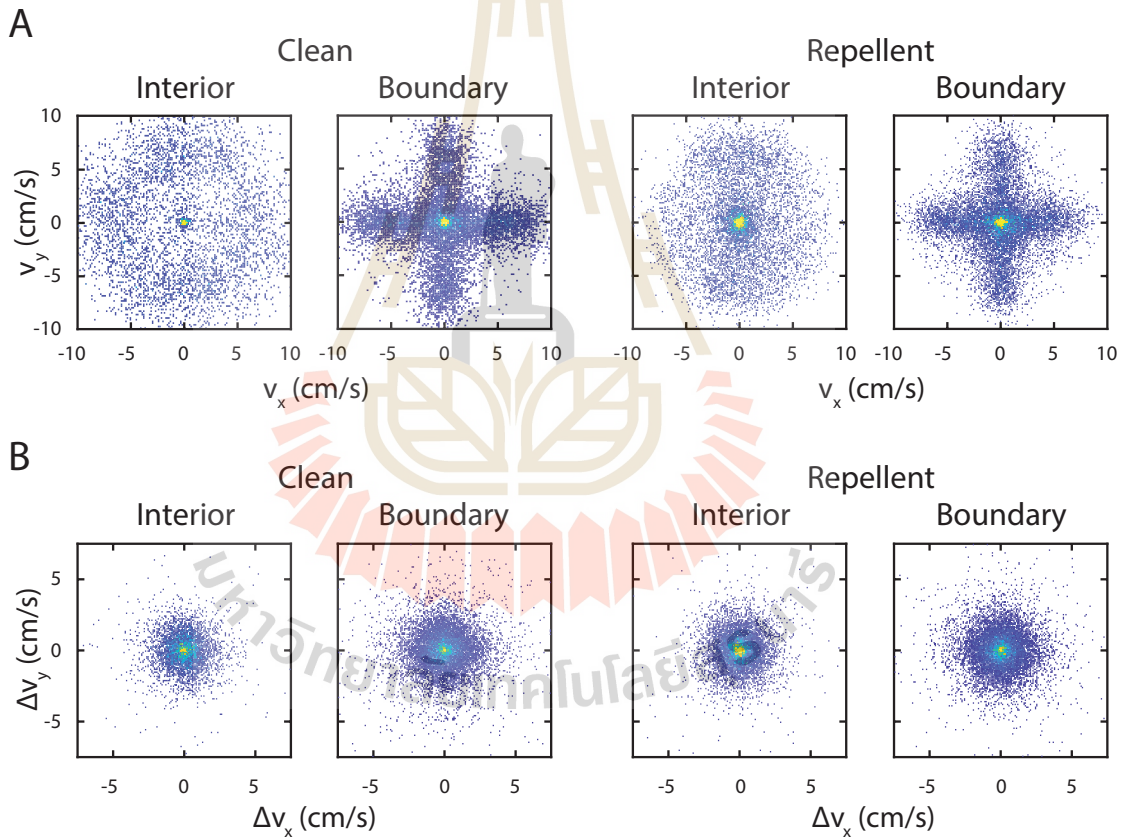
Figure 3.2 (A) Maps in velocity space, broken up by the ant position of Figure 2.4: the 'interior' data is more than 2 cm from arena boundary, while 'boundary' data is within this 2 cm strip. Left (right) plot is a clean (repellent of width $\ell = 10$ cm) experiment. **(B)** Ant velocity change maps in $(\Delta v_x, \Delta v_y)$ space for interior and boundary region.

3.2 Ants as Brownian particle

An analogy to Langevin theory of Brownian motion is used to model ant movement. The model ant experiences a total force $\mathbf{F}(t)$ that results in a change in velocity $\Delta \mathbf{v} = \mathbf{F}(t)\Delta t = (F_x(t), F_y(t))\Delta t$ with each time step. The velocity is taken to obey Newton's second law, for a unit mass, which is

$$\frac{\Delta \mathbf{v}}{\Delta t} \approx \frac{d\mathbf{v}}{dt} = \mathbf{F}(t) = \frac{\eta(t)}{\Delta t} - \frac{\mathbf{v}}{\tau} + \mathbf{E}. \tag{3.1}$$

The interaction of a Brownian particle with molecules in the ambient fluid results in a random impulse $\eta(t)$, with zero time average $\{\eta(t)\} = \{\eta\} = 0$, and a linear drag force with time-constant τ. We include these terms in the equation of motion for the ant: the random impulse because its precise motion is unpredictable and the drag force to keep the model stable.

The field $\mathbf{E} = \mathbf{E}(x, y)$ in Eq.3.1 accounts for an ant's interaction with any spatially dependent feature, such as the arena boundaries or chemical repellent. An appropriate model for the field must be chosen in each case. Since ants stop at arena boundaries, the boundary field can be described by a short-range repulsive force with a damping effect (like a normal force of a crash pad). For the chemical repellent, we define a potential energy $V(x, y)$ related to the field $\mathbf{E} = -\nabla V$ that indicates the desirability of a given position (the higher the potential the less desirable the position) and assign a positive potential to a position coated with repellent.

While Δv_x is proportional to the total force F_x, the normalized histogram in Figure 3.1B should be approximately proportional to the probability distribution function for η_x. This is mainly because the magnitude of η_x is larger than the impulse due to the other forces in Eq.3.1. The effect of the latter is further reduced by the square symmetry. A histogram bin contains position and velocity

components with both signs and the field is odd in x and y while the drag force is odd in v_x and v_y. In this way we can approximately disentangle the random and deterministic forces.

The histogram for either component of force, assumed equal to the probability density function (PDF) for the random local impulse $\eta = \eta_x$ or $\eta = \eta_y$, is fit to the following generalized Gaussian

$$p(\eta) = N exp\left(-\left[\frac{|\eta|}{c_m \sigma}\right]^m\right) \tag{3.2}$$

with the dimensionless number $c_m = \Gamma^{1/2}(1/m)\Gamma^{-1/2}(3/m)$ and the normalization factor $N^{-1} = 2c_m\sigma\Gamma(1 + 1/m)$ where $\Gamma(z)$ is the gamma function. Since, $p(\eta)$ is an even function, the mean $\{\eta\} = 0$ while the mean square is

$$\{\eta^2\} = \int_{-\infty}^{\infty} d\eta \eta^2 p(\eta) = \sigma^2. \tag{3.3}$$

So, σ is the standard deviation of the model distribution. A similar χ^2 goodness-of-fit is found over a range of values for σ and m (see Appendix A), so we fix $m = 1$, leaving σ as the only parameter. A Gaussian, with $m = 2$, does not give a good fit for any σ. The fits shown in Figure 3.2B have $m = 1$ and best-fit values of $\sigma_x^2 = 0.75 \pm 0.01$ (cm/s)^2 and $\sigma_y^2 = 0.70 \pm 0.01$ (cm/s)^2. (We denote by σ_x and σ_y the values of σ that give the best fit to the $p(\Delta v_x)$ distribution and $p(\Delta v_y)$ distribution, respectively.) It is the fact that Eq.3.2, with a single parameter σ, always provides an excellent fit to the measured distribution of velocity changes that makes it possible to model ant motion in a quantitative way using the Langevin approach.

In the model $\eta(t)$ is independently drawn at each time step. This ignores correlations between the random impulses at nearby times: an assumption, tested later, that is made here for simplicity. Also, with η_x and η_y drawn independently

and the field vector E_x, E_y assumed to respect square symmetry, the Cartesian components of Eq.3.1 are independent.

3.3 Measurable model properties

Using the general picture given above, we can calculate specific properties of model ant behavior that may be compared to measurements. Here, we sketch derivations of various ensemble averages of the model that can be compared to corresponding experimental values. More detailed derivations are given in the model calculation section.

3.3.1 Time-dependent squared velocity in the interior of a clean arena

First, we consider the mean-squared velocity of an ensemble of model ants. Write one component of the velocity as $v_x(t + \Delta t) = v_x(t) + \Delta v_x(t)$ and square this expression to obtain

$$v_x^2(t + \Delta t) - v_x^2(t) = 2v_x(t)\Delta v_x(t) + (\Delta v_x(t))^2. \tag{3.4}$$

The left side is Δt multiplied by $d/dt(v_x^2(t))$ while on the right side we use $\Delta v_x = \Delta t(dv_x/dt)$ and substitute Eq.3.1. Take an ensemble average of Eq.3.4 by averaging over many identical model ants with the same position and velocity at time t. An ensemble average is indicated by curly brackets. Different members of the ensemble experience different random impulses so $\{\eta\} = 0$. Random impulses affect $\{v_x^2\}$ via the term proportional to $\{\eta_x^2\} = \sigma^2$ that appears on the right side of Eq.3.4. This is larger than the deterministic terms, proportional to $(\Delta t)^2$, that

also appear. The ensemble-average is given by

$$\frac{d}{dt}\{v_x^2\} = \frac{\sigma^2}{\Delta t} - 2\frac{\{v_x^2\}}{\tau} + 2\{v_x E_x\} \tag{3.5}$$

where we dropped $(\Delta t)^2$ terms.

Eq.3.5 can be easily solved in the case of an infinite clean arena with $E = 0$ everywhere. The result is

$$\{v_x^2(t)\} = v_\infty^2 + (\{v_x^2(0)\} - v_\infty^2)e^{-2t/\tau} \tag{3.6}$$

where $v_\infty^2 = \sigma^2\tau/(2\Delta t)$. At large times, the system is in a stable state with a root-mean-square velocity component equal to v_∞ in an infinite arena.

In a finite arena, ants may not have enough space to achieve a speed v_∞ but, based on results in chapter IV, it appears that our arena is sufficiently large to do so. In fact, the shoulder features of the velocity distribution, Figure 3.1A, likely result from the fraction of the ant population that has achieved equilibrium. We use a rough estimate $v_\infty = 5.3$ cm/s, the center of the shoulder. A model ant disturbed by an arena boundary or other feature will wander away and forget its effects in time τ and distance τv_∞. It thereafter behaves like a member of an equilibrium ensemble in the infinite clean arena.

To obtain model predictions for Eq.3.6 in a finite arena, we must model the ant-boundary interaction. Perhaps the simplest plausible interaction is to have an ant stop abruptly at a boundary, with v_x going to zero at $x = -L/2$ while v_y is unaffected. Using such a crude model* we cannot accurately describe motion

---

*More serious modelling of the ant-boundary interaction is made difficult, in part, by the inhomogeneity of our boundary. Data indicate the interaction has a complex position, velocity dependence. The ant's interaction with our laboratory boundary is of no general interest, so we use the crude model and avoid quantitative discussion of near-boundary regions.

of ants near boundaries, but may be able to predict the ensemble average in the interior. So we define an interior region $|x| < L/2 - d, |y| < L/2 - d$, that excludes a boundary strip of width $d = 2$ cm.

Model ants stop at the boundary then move the short distance d to re-enter the interior, so an ant entering at $t = 0$ and $x = -L/2 + d$ has a small initial velocity $v_x(0)$. Its velocity $v_y(0)$ is not small because the $x = -L/2$ boundary does not affect it. The average squared-velocity $\{v_x^2(t)\} = \{v_\perp^2(t)\}$ perpendicular to the boundary and $\{v_y^2(t)\} = \{v_\parallel^2(t)\}$ can then be calculated using Eq.3.6.

These time-dependent squared velocities can be readily compared to experiment. We compile data segments with an ant entering the interior at time t_1 and exiting with time t_2. Substituting t_1 from t, we have an experimental ensemble of ants entering the interior at $t = 0$. It is a large ensemble because each ant will enter and exit the interior region many times.

3.3.2 Position dependence of squared velocities with and without repellent

The model predicts that an ensemble-averaged squared velocity depends on position. Ants that move away from a disturbance approach the equilibrium state of an infinite arena, so $\{v_x^2\}$ and $\{v_y^2\}$ approach v_∞^2. For the clean arena, $\{v_x^2\}$ is small near $x = \pm L/2$ and approaches v_∞^2 deep in the interior. With repellent present, ant velocity receives a negative (positive) impulse as they enter (leave) zone $\mathcal{R}$. Away from these disturbance at the borders of zone $\mathcal{R}$, the squared velocity again approaches v_∞^2.

To test the predicted position-dependence against the data, we take the full dataset and arrange it in order of increasing x before taking a running average of v_x^2 and v_y^2. In this way, we get x-dependent squared-velocities.

3.3.3 Field and potential

The field **E** in Eq.3.1 comes from the arena boundaries and chemical repellent. The arena boundary has the effect of keeping ants in the arena, so the associated field is a strong, short-range field acting inward and normal to the boundary. It could be modelled by an infinite potential barrier, with a damping effect used to avoid billiard-ball reflections.

The potential associated with the repellent $V(x, y)$ has a corresponding field $\mathbf{E}(x, y) = -\nabla V(x, y)$. The model potential $V(x)$ is a square barrier, with height V_0 and width ℓ. The resulting field has an x component

$$E(x) = V_0[-\delta(x + \ell/2) + \delta(x - \ell/2)]. \tag{3.7}$$

and no y-component. An ant that moves into zone $\mathcal{R}$ has to overcome a potential barrier. If it exits a clean zone with velocity $v_x = v_1$ then it has a reduced velocity $v_x = \sqrt{v_1^2 - 2V_0}$ in zone $\mathcal{R}$. Model ants with a velocity less than $v_{min} = \sqrt{2V_0}$ cannot enter zone $\mathcal{R}$.

Experimental values for the field $E(x)$ and potential $V(x)$ can be measured in the following way. When we arrange the data in order of increasing x and take a running average of Δv_x, we have Δv_x as a function of position x, known to within bin width Δx. The values of (t, y, v_x, v_y) vary within each bin and the bin-average of η_x is zero. The drag force is not required by symmetry to average to zero but it turns out to be negligible. Thus, the running average of Δv_x is equal to $E_x(x)$. This is the field measurement. The integral $V(x) = -\int dx E(x)$ with $V(x) = 0$ outside zone $\mathcal{R}$ gives the potential.

3.3.4 Crossing probability and residence time

A model ant, after having entered zone $\mathcal{R}$, has a probability P_C to proceed through it, rather than turn back to the zone from which it came. The average time it resides in zone $\mathcal{R}$ before leaving to either side is T_R. In model calculation section-section 3.4.2, we calculate these quantities for the model, assuming the ensemble arriving at the border is in equilibrium. When we do the calculation for a clean arena, we take the potential $V_0 = 0$. Both quantities can be measured by selecting the relevant data subset, i.e. finding all instances where the ant enters zone $\mathcal{R}$ at time t_1 and then determining the time t_2 when it exits that zone and noting to which side.

3.4 Model calculation

Here, we more fully develop the model sketched in the previous section and use it to calculate several measurable properties of ant motion. These are all ensemble averages, which can be approximated without using simulations of the random motion. Because of the square symmetry of the arena, the motion along x and y are independent. So, most quantities can be obtained with a one-dimensional picture. The generalization to two-dimensions, where needed, is straightforward.

3.4.1 Ants in a clean arena

Consider a large ensemble of ants moving in one dimension with their velocity determined by one component of Eq.3.1. The ensemble has a probability distribution function $\Pi(x, v, t)$ over position x, velocity v, at time t. A normalized probability distribution over position (velocity) alone is obtained by integrating $\Pi(x, v, t)$ over
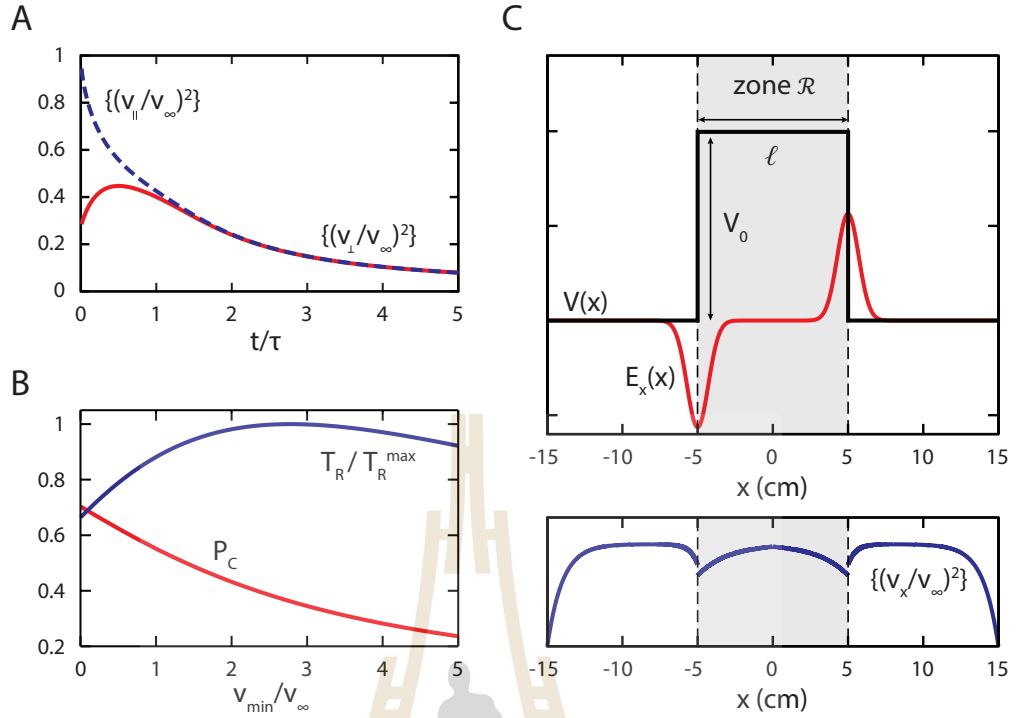
Figure 3.3 Model predictions. **(A)** plot of $\{v_x^2\}$ (red solid curve) and $\{v_y^2\}$ (blue dashed curve) for ants in the interior region versus time. Ants entered the interior near arena boundary at $x = -L/2$ so the x direction is perpendicular, and y parallel to this boundary. Time is in units of τ, velocity is in units v_∞. **(B)** The probability P_C that the ant crosses zone $\mathcal{R}$ (width $l = 10$ cm) and time T_R spent continuously in zone $\mathcal{R}$, normalized to its maximum $T_R^{\max}$, are plotted versus v_{min}/v_∞. The parameter $v_{min}^2 = 2V_0$ where V_0 is the height of the potential barrier presented by the chemical repellent in zone $\mathcal{R}$. **(C)** The potential $V(x)$ versus position, showing V_0 in zone $\mathcal{R}$ and the resulting field $E_x(x) = -dV/dx$ and the effect on squared velocity. The vertical scale is arbitrary.

all velocity (position). The average of a function $f(x, v, t)$ at time t is

$$\{f(t)\} = \int_{-\infty}^{\infty} dx \int_{-\infty}^{\infty} dv \Pi(x, v, t) f(x, v, t). \tag{3.8}$$

Of particular interest are mean values $\{x(t)\}$, $\{v(t)\}$ and variances

$$\sigma_x^2(t) = \{x^2(t)\} - \{x(t)\}^2, \quad \sigma_v^2(t) = \{v^2(t)\} - \{v(t)\}^2. \tag{3.9}$$

Suppose that each member of an ensemble begins with $x(0) = x_0$, and $v(0) = v_0$ in an infinite, clean arena. The velocity and position change as

$$v(t + \Delta t) = v(t) - \frac{v(t)\Delta t}{\tau} + \eta(t) \tag{3.10}$$

$$x(t + \Delta t) = x(t) + v(t)\Delta t, \tag{3.11}$$

where $\eta(t)$ is a random variable, with the probability distribution $p(\eta) = p(-\eta)$. Thus $\{\eta\} = 0$ and $\{\eta^2\} \equiv \sigma^2$ where σ is the standard derivation of random impulses. In an ensemble average, terms odd in η vanish, so

$$\{v(t + \Delta t)\} - \{v(t)\} = -\frac{\{v(t)\}\Delta t}{\tau}. \tag{3.12}$$

In the $\Delta t \to 0$ limit, this becomes

$$\frac{d}{dt}\{v\} = -\frac{\{v\}}{\tau}. \tag{3.13}$$

In the same way, we find

$$\frac{d}{dt}\{v^2\} = -\frac{2\{v^2\}}{\tau} + \frac{\sigma^2}{\Delta t}, \tag{3.14}$$

$$\frac{d}{dt}\{xv\} = -\frac{xv}{\tau} + \{v^2\}, \tag{3.15}$$

$$\frac{d}{dt}\{x\} = \{v\}, \tag{3.16}$$

$$\frac{d}{dt}\{x^2\} = 2\{xv\} \tag{3.17}$$

that can all be integrated. The solutions are

$$\{v(t)\} = v_0 e^{-t/\tau}, \tag{3.18}$$

$$\{v^2(t)\} = v_\infty^2 + (v_0^2 - v_\infty^2)e^{-2t/\tau}, \tag{3.19}$$

$$\{x(t)v(t)\} = \tau v_\infty^2 + (x_0 v_0 + \tau v_0^2 - 2\tau v_\infty^2)e^{-t/\tau} - \tau(v_0^2 - v_\infty^2)e^{-2t/\tau}, \tag{3.20}$$

$$\{x(t)\} = x_0 + v_0 \tau (1 - e^{-t/\tau}), \tag{3.21}$$

$$\{x^2(t)\} = x_0^2 + 2\tau v_\infty^2 t + 2\tau(x_0 v_0 + \tau v_0^2 - 2\tau v_\infty^2)(1 - e^{-t/\tau})$$

$$-\tau^2(v_0^2 - v_\infty^2)(1 - e^{-2t/\tau}). \tag{3.22}$$

We introduce a terminal velocity $v(t \to \infty) \equiv v_\infty$ defined by $v_\infty = \sigma^2 \tau/(2\Delta t)$. Velocity will be written in units of v_∞, time in units of τ, and distance in units of τv_∞. So, all three variables are dimensionless and the solution becomes

$$\{v^2(t)\} = 1 + (v_0^2 - 1)e^{-2t}, \tag{3.23}$$

$$\{x(t)v(t)\} = 1 + (x_0 v_0 + v_0^2 - 2)e^{-t} - (v_0^2 - 1)e^{-2t}, \tag{3.24}$$

$$\{x^2(t)\} = x_0^2 + 2t + (2x_0 v_0 + 2v_0^2 - 4)(1 - e^{-t})$$

$$-(v_0^2 - 1)(1 - e^{-2t}). \tag{3.25}$$

The mean values are

$$\bar{v}(t, v_0) = \{v(t)\} = v_0 e^{-t}, \tag{3.26}$$

$$\bar{x}(t, x_0, v_0) = \{x(t)\} = x_0 + v_0(1 - e^{-t}) \tag{3.27}$$

where variances given by

$$\sigma_v^2(t) = 1 - e^{-2t}, \quad \sigma_x^2(t) = -3 + 2t + 4e^{-t} - e^{-2t}. \tag{3.28}$$

At large t, the spread in velocity $\sigma_v(t) \to 1$ while σ_x increases without bound in an infinite arena. Note that, after a time $t \approx \tau$, an ant forgets its initial state and approaches its equilibrium velocity. After moving a distance $d \approx \tau v_\infty$ away from a disturbance, it similarly approaches equilibrium.

We will write $G(x; \bar{x}, \sigma)$ for a normalized Gaussian in the variable x, with the mean $\bar{x}$ and standard deviation σ. The initial distribution can then be written $\Pi_0(x, v) = \Pi(x, v, 0) = \delta(x - x_0)\delta(v - v_0) = G(x; x_0, \epsilon)G(v; v_0, \epsilon)$ using a particular representation of a delta function with an infinitesimal quantity ϵ. The equilibrium distribution for the infinite arena is $\Pi(x, v, \infty) = \Pi_\infty(v) = G(v; 0, 1)$. To approximate time-evolution of an ensemble, replace Gaussian parameters with time-dependent values that give the mean and standard deviation found above. Thus, the time-dependent distribution is

$$\Pi(x, v, t) = G(x; \bar{x}(t, x_0, v_0), \sigma_x(t))G(v; \bar{v}(t, v_0), \sigma_v(t)) \tag{3.29}$$

when $\Pi_0(x, v) = \delta(x - x_0)\delta(v - v_0)$. An arbitrary initial distribution is first written as

$$\Pi_0(x, v) = \int_{-\infty}^{\infty} dx' \int_{-\infty}^{\infty} dv' \Pi_0(x', v')G(x; x', \epsilon)G(v; v', \epsilon) \tag{3.30}$$

and primed variables treated as initial values, to get

$$\Pi(x, v, t) = \int_{-\infty}^{\infty} dx' \int_{-\infty}^{\infty} dv' \Pi_0(x', v')$$

$$G(x; \bar{x}(t, x', v'), \sigma_x(t))G(v; \bar{v}(t, v'), \sigma_v(t)). \tag{3.31}$$

In two dimensions, the distribution functions is $\Pi(x, v_x, t)\Pi(y, v_y, t)$ and Eq.3.31

generalized to include integrals over y', v'_y with two more Gaussians of the same form.

The results above apply to a clean, infinite arena. The effect of the field, which is important at arena boundaries and at the borders to zone $\mathcal{R}$ when the chemical repellent is present, will be treated as initial values of these equations. The simplest model of the interaction at arena boundaries is to have ants stop abruptly at the boundary and forget their previous motion. When the ant reaches the boundary at $x = \pm L/2$, its velocity v_x drops to zero while its motion in the y direction is unaffected. For a clean arena that is sufficiently large, i.e. $L >> 1$ (in units of τv_∞), ants far from boundaries are in equilibrium.

First consider the time-dependence of the squared velocity of ants in the clean arena that have entered the interior region, which is a square of length $L' = L - 2d$ centered in the arena of length L where $d << L$. An ant starting at the boundary $x = -L/2$ with $v_x = 0$ needs a typical time $t = t_1$ to reach the interior region, which is found by inverting $\{x^2(t_1)\} = d^2$. The standard deviation of velocity at this time is $\sigma_1 = \sigma_v(t_1) << 1$. Only ants with $v_x > 0$ enter the central region from the side, so, we use $G_+(x; , \bar{x}, \sigma) = 2\theta(x)G(x; \bar{x}, \sigma)$ with

$$\theta(x) = \begin{cases} 1 & \text{where } x > 0, \\ 0 & \text{where } x < 0 \end{cases} \tag{3.32}$$

to write the distribution for members entering at $t = 0$ as $\Pi(x, v_x, 0) = \delta(x + L'/2)G_+(v_x; 0, \sigma_1)$. For motion along y we assume that most ants, being far from boundaries $y = \pm L/2$, are in equilibrium, so, $\Pi(y, v_y, 0) = (1/L')\theta(L'/2 -$

$|y|)G(v_y; 0, 1)$. The time-evolution is introduced via Eq.3.31 and

$$\{v_\alpha^2(t)\} = \int_{-L'/2}^{L'/2} dx \int_{-L'/2}^{L'/2} dy \int_{-\infty}^{\infty} dv_x \int_{-\infty}^{\infty} dv_y$$

$$v_\alpha^2 \Pi(x, v_x, t) \Pi(y, v_y, t) \tag{3.33}$$

where $\alpha = x, y$. The results of Eq.3.33 were shown in Figure 3.3C. At small times, $\{v_x^2(t)\}$ increases because ants accelerate as they move away from the boundary. After a time of order τ, it reaches a peak, some fraction of v_∞^2, then starts to decrease. Members that leave the central region are removed from the ensemble and, since fast ones leave first, $\{v_x^2(t)\}$ decreases. In contrast, the initial value $\{v_y^2(0)\} = v_\infty^2$ is maximal, so, $\{v_y^2(t)\}$ decreases monotonically.

3.4.2 Ants with the potential barrier

Next, we introduce the chemical repellent to the central zone $\mathcal{R}$, defined by $|x| < \ell/2$ where $\ell < L$, which adds a field $E_x(x) = -dV/dx$ to Eq.3.1. The effective potential

$$V(x) = \begin{cases} V_0 & \text{in zone } \mathcal{R}, \\ 0 & \text{elsewhere.} \end{cases} \tag{3.34}$$

After encountering the step potential, an ant crosses into zone $\mathcal{R}$, every member receives a negative impulse $\Delta v_x = -v_{min} = -2\sqrt{V_0}$ opposite to the direction of its velocity. The potential results in a reduced density of ants in zone $\mathcal{R}$, since some are prevented from entering the zone.

Consider an ensemble approaching the border to zone $\mathcal{R}$. Since this border is far from the arena boundaries, we assume the distribution is in equilibrium upon arrival at the border. While crossing into zone $\mathcal{R}$, some members are repelled by the barrier and the rest have their velocity reduced by v_{min}. The resulting distribution, just after arriving into zone $\mathcal{R}$ at $x = -\ell/2$ is $\Pi_0(x, v_x) = \delta(x +$

$\ell/2)\theta(v_x)G(v_x+v_{min};0,1)$. This ensemble, which lost some members at the border, has to be normalized.

To calculate the crossing probability P_C and residence time T_R, we first find these quantities $P_C(x, v_x)$ and $T_R(x, v_x)$ for an ant with a certain initial position x and certain velocity v_x. These functions can be weighted with the initial distribution to estimate their measurable values. Thus, the expected crossing probability is

$$P_C = \int dv_x \Pi_0(-\frac{\ell}{2}, v_x) P_C(-\frac{\ell}{2}, v_x) \tag{3.35}$$

and residence time is

$$T_R = \int \Pi_0(-\frac{\ell}{2}, v_x) T_R(-\frac{\ell}{2}, v_x) \tag{3.36}$$

where we are using a one-dimensional picture for simplicity.

A function $F(x, v_x)$ that depends on the initial values $x(0) = x$ and $v_x(0) = v_x$ can be set equal to its ensemble average one time step later, so

$$P_C(x, v_x) = \{P_C(x(\Delta t), v_x(\Delta t))\} \tag{3.37}$$

$$T_R(x, v_x) = \Delta t + \{T_R(x(\Delta t), v_x(\Delta t))\frac{t}{\tau} + \eta\} \tag{3.38}$$

and then either function written as

$$F(x(\Delta t), v_x(\Delta t)) = F(x + v_x\Delta t, v_x - v_x\frac{\Delta t}{\tau} + \eta). \tag{3.39}$$

We Taylor-expand in Δt

$$F(x(\Delta t), v_x(\Delta t)) = v_x\Delta t(\frac{\partial F}{\partial x} - \frac{1}{\tau}\frac{\partial F}{\partial v_x}) \tag{3.40}$$

and drop terms odd in η from the ensemble average. The first order terms $v_x\Delta t(\partial F/\partial x - \tau^{-1}(\partial F/\partial v_x))$ vanish if the function depends on a single variable,

$F(x, v_x) = F(r)$ with $r = x + v_x \tau$. Most of the second order terms similarly cancel. The surviving term up to second order results in

$$\frac{\partial^2 P_C}{\partial r^2} = 0, \tag{3.41}$$

$$\frac{\partial^2 T_R}{\partial r^2} = -1 \tag{3.42}$$

in dimensionless variables. In writing the solution,

$$P_C(r) = \alpha_1 r + \alpha_2, \tag{3.43}$$

$$T_R(r) = -\frac{1}{2}r^2 - \beta_1 r + \beta_2. \tag{3.44}$$

With boundary conditions $P(-\ell/2, 0) = T(-\ell/2, 0) = T(\ell/2, 0) = 0$ and $P(\ell/2, 0) = 1$. Then, the coefficients are $\alpha_1 = 1/\ell, \alpha_2 = 1/2, \beta_1 = 0, \beta_2 = \ell^2/8$. We find

$$P_C(-\frac{\ell}{2}, v_x) = P_C(v_x) = \frac{v_x \tau}{\ell}, \tag{3.45}$$

$$T_R(-\frac{\ell}{2}, v_x) = T_R(v_x) = \frac{v_x \tau}{2}(\ell - v_x \tau). \tag{3.46}$$

These expressions are small-velocity approximations, because of the Taylor expansion, and evidently meaningless for $v > \ell$. To crudely treat large velocities, we can set the crossing probability to one and residence time to zero for $v_x > \ell$.

Since $P_C(v_x)$ is a monotonically increasing function of v_x, with the slowest ants having no chance to successfully crossing zone $\mathcal{R}$. The effect of the potential barrier is to reduce the typical initial velocity v_x and thus decrease P_C. The function $T_R(v_x)$ is non-monotonic. It increases with velocity at small v_x, because slightly-faster ants penetrate further into zone $\mathcal{R}$, so, it takes them longer to retreat back. It decreases at large v_x because the fastest ants race through zone $\mathcal{R}$ in less time. There is a corresponding non-monotonic dependence of T_R on the

potential barrier height. Consequently, a weak barrier potential V_0 will result in ants spending more time in zone $\mathcal{R}$, then, they would if $V_0 = 0$. That is, according to this model, ants will spend more time in a region with a mild repellent present than they would in a clean region of the same size.

Note that, the quantitative value of P_C, obtained from this model, is considerably lower than the measured value-likely because of the significant effect that the boundaries at $y = \pm L/2$ have on the latter. The qualitative effect, illustrated in Figure 3.3, is indicated by a plot of T_R normalized to its maximum value versus v_{min}.

Finally, consider the dependence of the average velocity squared $\{v_x^2\}$ on position x in equilibrium (i.e. the time average of this quantity). It is obtained using Eq.3.8 with $\Pi(x, v_x, t)$ set equal to the equilibrium distribution. Again, we seek only a qualitative result. Since the equilibrium distribution does not change with time, it satisfies

$$v_x \frac{\partial \Pi}{\partial x} + \frac{\partial v_x}{\partial t} \frac{\partial \Pi}{\partial v_x} = 0. \tag{3.47}$$

To simplify the problem, we use a weak-field limit and assume the distribution is close to the zeros-field equilibrium, $\Pi_\infty(v_x)$ so $\Pi(x, v_x) = \Pi_\infty(v_x) + \Pi_1(x, v_x)$ where the second term, absent were it not for the field, is small. Equation 3.47 becomes

$$\frac{\partial \Pi_1}{\partial x} - E(x)\Pi_\infty(v_x) - \frac{\partial \Pi_1}{\partial v_x} = 0. \tag{3.48}$$

where we dropped terms odd in η, used $v_x^2 = 1$ in the long time limit, and ignored terms $E(x)\Pi_1(x, v_x)$ second order in the weak field. The field due to the repellent is

$$E(x) = V_0[-\delta(x + \ell/2) + \delta(x - \ell/2)]. \tag{3.49}$$

It cause step-like jumps in the distribution $\Pi_1(\ell/2, v_x)$ at the borders to zone $\mathcal{R}$. Integrating Eq.3.48 over a small region at the border between the clean and the

repellent zone (zone $\mathcal{R}$) gives

$$\int_{-\ell/2-\epsilon}^{-\ell/2+\epsilon} dx \frac{\partial \Pi_1}{\partial x} = \Delta \Pi_1(-\frac{\ell}{2}, v_x) = -V_0 \Pi_\infty(v_x). \tag{3.50}$$

This is a localized disturbance caused by the field. As we move into the zero-field region $\Pi_1(x, v_x)$ decays to zero and $\{v_x^2(x)\}$ approaches one.

The zero-field version of Eq.3.48 is satisfied by any function $\Pi_1(x, v_x) = \Pi_1(x + v_x)$, so a possible form

$$\Pi_1(x, v_x) = exp(-\kappa[x + v_x - x_0])\Pi_1(x_0) \tag{3.51}$$

decays as we move away from a disturbance at x_0. Ants moving out of zone $\mathcal{R}$ receive an initial burst due to the force from the repellent and have a correspondingly larger slope κ. The distribution at the boundaries is $\Pi(-L/2, v_x) = \Pi(L/2, v_x) = \delta(v_x)$. We treat this as another localized disturbance that decays. This qualitative behavior was sketched in Figure 3.3.

CHAPTER IV

ANT'S BEHAVIOR

In this chapter, we discuss our application of Langevin theory to the motion of individual weaver ants. It turns out that both the random and deterministic components of the forces assumed in Langevin theory can be seen in the data. The probability distribution function of random impulses is robust and characterized by a single parameter. The deterministic response to chemical repellent can be adequately modelled by a potential energy that indicates the desirability of a given position. The theory explains most qualitative properties of the statistical data. Semi-quantitative agreement between theory and data is also achieved. The mathematical simplicity of the model, which allows a full characterization of navigation with a small number of parameters, suggests that it is an appropriate starting-point for further quantitative studies, including those aimed to better understand the ant's communication.

4.1 Experimental Results

4.1.1 The distribution of random impulses

The most basic quantity to measure and analyze is the probability distribution function of velocity changes Δv_x and Δv_y. According to Langevin-based model, Eq.3.1 describes the distribution of random local impulses η_x that have a dominant influence on probability distribution for Δv_x. In this section, we will try to fit the measured $p(\Delta v_x)$ to Eq.3.1 with a single parameter σ.
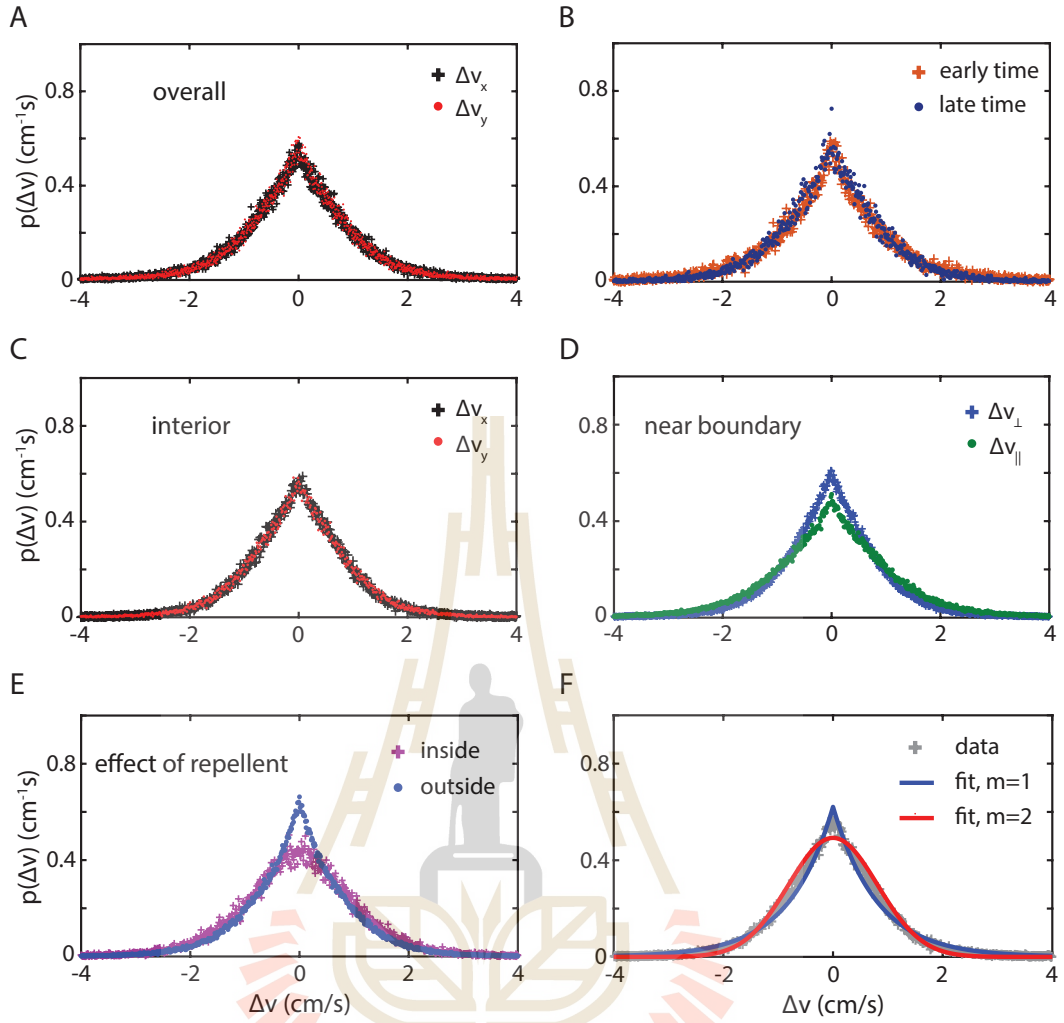
Figure 4.1 The measured probability distribution function $p(\Delta v)$ obtained for various data subsets are compared, including **(A)** average overall data in a clean arena. **(B)** Comparing Δv_x measured for "Early" and "Late" time. **(C)** "Interior", Δv_x and Δv_y for ants at least $d = 2$ cm from any boundary. **(D)** Δv_x measured for $|x| > L/2 - d$ ($\Delta v_{\parallel}$) and $|y| > L/2 - d$ ($\Delta v_{\perp}$) to the arena for ants within 2 cm. **(E)** Comparing Δv_x for "In" and "Out" of the repellent when the width $\ell = 10$ cm. **(F)** The probability distribution $p(\Delta v_x)$ in a clean arena compared to the probability distribution function indicated in Eq.3.2 with $m = 1$ (blue) and the Gaussian $m = 2$ (red).

In doing these fits, we are attributing $p(\Delta v_x)$ wholly to random impulses. This gives a good fit in most cases but it is not consistent with the model. The model says that $p(\Delta v_x)$ is affected by deterministic forces (the field and drag force) as well as random impulses. When we fit $p(\Delta v_x)$ to Eq.3.2 we are burying deterministic effects into changes in σ. Still, this is a reasonable approach because i/ random and deterministic force components are entangled and ii/ the random impulses are bigger.

Recall that, if $p(\Delta v_x)$ was determined entirely by the random impulses, the size of σ would indicate how erratic ant motion is. So a larger value of σ means, according to our theoretical model, either that random impulses are getting stronger or deterministic effects are significant. We will return to do a better job of isolating deterministic forces in later sections.

Eq.3.1 was used in fits to distributions $p(\Delta v_x)$, $p(\Delta v_y)$ for several subsets of the data, with results shown in Figure 4.1 and Table 4.1. The subsets are: "Overall" (data for all ants at all times and positions in the clean arena), "Early" and "Late" (all positions in the clean arena at time $0 < t \leq 30$ s and $270 < t \leq 300$ s, respectively), "Interior" (all times in the clean arena with position $|x| < L/2 - d$, $|y| < L/2 - d$ at least $d = 2$ cm from any boundary) along with the complementary subsets for positions $|x| > L/2 - d$ and $|y| > L/2 - d$ within d from the boundaries. Finally, with the repellent coated over zone $\mathcal{R}$, length $\ell = 10$ cm and $\ell = 2.5$ cm, we show results for positions "In" and "Out" of this repellent. For "In" we used the data subset in which the ant entered zone $\mathcal{R}$ with position $|y| < L/2 - d$ to reduce the boundary effects.

The first observation is that the distributions are qualitatively robust. Quantitatively, these values indicate a good fit and, as evident from Figure 4.1, describes a fit that appears excellent to the eye. The size of σ^2 is also roughly

Table 4.1 The results of fitting the measured distribution of velocity changes $p(\Delta v_x)$ and $p(\Delta v_y)$ for various data subsets to Eq.3.1 with $m = 1$. The labels "Early/late" refer to times $0 < t \leq 30$ s and $270 < t \leq 300$ s, while "Interior" means $|x| < L/2 - d, |y| < L/2 - d$ and $x \approx L/2$ means $L/2 - d \leq |x| < L/2$. When repellent is present in zone $\mathcal{R}$, with width ℓ in cm, the "In" label means $|x| < \ell/2$, "Out" means $|x| > \ell/2$ and $x \approx 0$ means $|x| < 1.25$ cm. The fitting parameter σ^2 had an uncertainty of about 0.01 $\mathrm{(cm/s)}^2$ for most subsets, but was somewhat higher for others, with a maximum 0.09 $\mathrm{(cm/s)}^2$ in the repellent for $\ell = 2.5$ cm. The dimensionless Pearson correlation coefficient was calculated to the nearest 10^{-2}.

Subset	$p(\Delta v_x)$			$p(\Delta v_y)$		
	$\sigma_x^2 \mathrm{(cm/s)}^2$	χ^2	$10^2\rho$	$\sigma_y^2 \mathrm{(cm/s)}^2$	χ^2	$10^2\rho$
Overall	0.75	2	-2	0.70	2	-1
Early	0.78	8	0	0.77	10	0
Late	0.68	16	1	0.63	12	2
Interior	0.65	3	-4	0.67	3	-4
$|x| \approx L/2$	0.69	3	0	1.04	2	2
$|y| \approx L/2$	0.92	1	1	0.56	2	-1
$\ell = 10$, In	0.93	4	1	0.74	18	-2
$\ell = 10$, $x \approx 0$	0.97	2	-1	0.73	2	1
$\ell = 10$, Out	0.58	2	-1	0.62	2	-1
$\ell = 2.5$, In	1.31	1	4	0.90	3	2
$\ell = 2.5$, Out	0.76	22	-2	0.84	19	-1

constant across all data sets. This indicates that the deterministic effects are not strong enough to completely destroy agreement between Eq.3.2 and the $p(\Delta v_x)$

data. Also, the Pearson correlation coefficient, $\rho << 1$ in all cases. This means that impulses at different time steps are approximately independent. The dimensionless χ^2, indicating goodness-of-fit, was calculated to the nearest 1.

The correlation coefficients, for several data subsets, are $\rho = \rho(\Delta v_x(t), \Delta v_x(t + 3\Delta t))$ and $\rho = \rho(\Delta v_y(t), \Delta v_y(t + 3\Delta t))$ in respective columns, where

$$\rho(X, Y) = \frac{\{(X - \{X\})(Y - \{Y\})\}}{\sqrt{\{X^2\} - \{X\}^2}\sqrt{\{Y^2\} - \{Y\}^2}} \qquad (4.1)$$

and the curly brackets denote an average over the subset. We considered times separated by $3\Delta t$ because those closer together are constructed using overlapping data point $\mathbf{r}(t)$. Since $\{\Delta v_x(t)\} = \{\Delta v_x(t + 3\Delta t)\} \approx 0$ and $\{(\Delta v_x(t))^2\} = \{(\Delta v_x(t + 3\Delta t))^2\} \approx \sigma^2$, the value of $\rho = \{\Delta v_x(t)\Delta v_x(t + 3\Delta t)\}/\sigma^2$ indicates the size of the correlation of impulses at nearby time steps compared to their magnitude at each step. The fact that $\rho << 1$ suggest that it is reasonable to treat the random impulses as uncorrelated.

Quantitatively, differences are seen in the parameters of Table 4.1. First, the square symmetry is not perfect, since σ_y is smaller than σ_x. The most likely explanation for this effect is that ants alter their motion according to their vision, or some other long-range perception. While the effect is much larger than that predicted by chance (the difference between σ_x^2 and σ_y^2 is five times larger than uncertainty, which is 0.01 $(\text{cm/s})^2$ for both), it is still small enough that it does not seriously threaten the assumption that the navigation is local. Other sources of variation in σ^2 are discussed next.

4.1.2 Time and position dependence of random motion

According to Table 4.1 and Figure 4.2, σ values decrease modestly with time t. The deterministic forces are time-independent so this effect can be safely attributed to

real changes in the random impulses. The effect is further detailed in Table 4.2, which presents the results of linear fits to σ versus t.
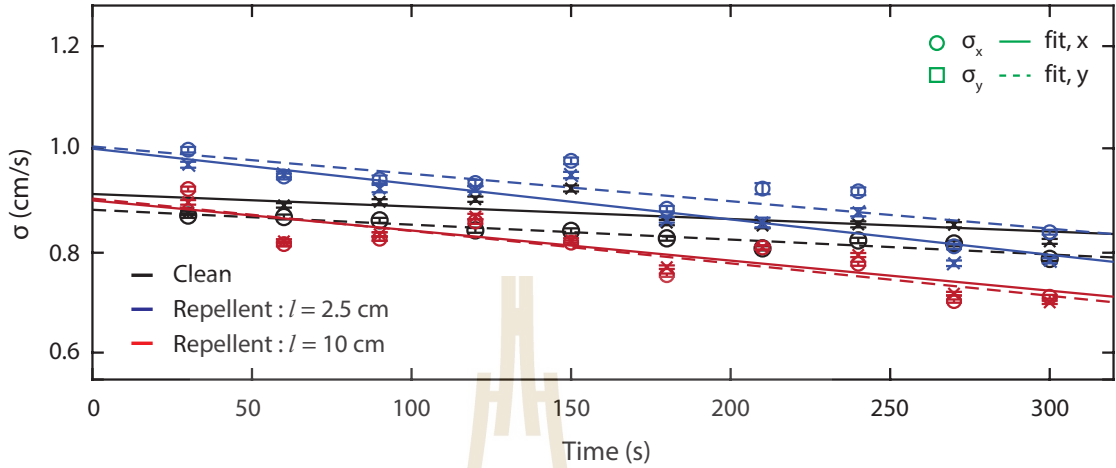
Figure 4.2 The σ_x (circle) and σ_y (square) change over time for all ants in a clean arena (black) and the repellent experiment, $l = 2.5$ cm (blue) and $l = 10$ cm (red). The σ values decrease slightly with time.

For a clean arena, the downward trend of σ with t is weak: the slope of σ_y versus t is zero within uncertainty. In an arena with repellent, σ decrease more significantly since the slope is several times larger than its uncertainty. This could be an indication that ants learn to move a bit more cautiously, i.e. less erratically, over time in the presence of repellent. But the main point here is that σ does not change substantially over the duration of the experiment.

Also from Table 4.1, there is a sizeable difference in the value σ^2 obtained for positions near boundaries compared to those for the interior. While the difference is an order of magnitude larger than the uncertainty in σ^2, it is certainly affected by the effect of the ant-boundary interaction on the distributions $p(\Delta v_x)$, $p(\Delta v_y)$ near the boundary. The interaction is complicated* and boundary effects, being peculiar to our arena design, are of no general interest so we do not attempt

Table 4.2 A linear regression was done on the data Figure 4.2, in which σ values are plotted versus time t. The slope $m = \Delta\sigma/\Delta t$ and its uncertainty are indicated for σ obtained from Δv_x and Δv_y in the clean arena and that with repellent present.

Linear curve fitting	$10^3 m_{\sigma,x}$ (cm/s^2)	$10^3 m_{\sigma,y}$ (cm/s^2)
Clean	-0.2±0.1	-0.3±0.0
$l = 2.5$ cm	-0.7±0.1	-0.5±0.1
$l = 10$ cm	-0.6±0.1	-0.6±0.1

detailed modelling[‡].

Finally, the value of σ is larger in zone $\mathcal{R}$ when repellent is present. Again the difference is far greater than the statistical uncertainty in σ^2. If the fit value of σ could be wholly attributed to random impulses, then an enhancement of σ would be interesting in light of what is known about chemotaxis by bacteria and other organisms. Bacteria that move according to the "run and tumble" technique vary the frequency at which they tumble depending on the local environment (Bialek, 2012; Macnab and Koshland, 1972; Szurmant and Ordal, 2004; Shimizu et al., 2010; Long et al., 2017). Perhaps ants also modify their random walk behavior, by adjusting σ, when they find themselves in a hostile region. However, such behavior is not evident from the data. Rather, it appears that the most significant response of ants to the repellent is an initial velocity drop, well-described by the Langevin/Newtonian picture and discussed below.

_____

[‡]A plausible reason why ants tend to remain near boundaries is that a one-dimensional structure like this allows an ant to explore a large region without becoming disoriented: humans would likely use the same strategy, following the river to avoid walking in circles. It is a large effect, from $\{v_x^2\}$ and $\{v_y^2\}$ plots in Figure 4.3 appears that ants move at high speed along the boundary and are subject to large impulses parallel to the boundary as they do so.

In Figure 4.1E, showing data obtained within the repellent, we see an apparent qualitative difference between the measured probability distribution and Eq.3.2 with $m = 1$. Indeed, the experimental curve looks similar to a Gaussian with $m = 2$. If we nevertheless fit the data using $m = 1$, then we obtain a relatively large σ. We should be cautious in taking the value seriously. Ants in the repellent have recently encountered the potential step as the entered zone $\mathcal{R}$. So, Figure 4.1E is probably strongly affected by field effects. Because of this complication, we cannot confidently discuss chemotaxis effects on random motion. We turn now to deterministic effects, which are clearer.

4.1.3 Deterministic motion

4.1.3.1 Time-dependent squared velocity

The model prediction of the squared velocity $\{v_x^2\}$ and $\{v_y^2\}$ among an ensemble of ants that entered the interior of a clean arena, defined by $|x| < L/2 - d, |y| < L/2 - d$ where $d = 2$ cm, at time $t = 0$ s is shown in Figure 4.3. Here $v_\parallel$ is the velocity component parallel to the boundary strip from which the ant entered and $v_\perp$ is perpendicular to it. The initial value of $\{v_\perp^2\}$ is small, since members recently stopped at the boundary, but $\{v_\parallel^2\}$ is larger because ants move rapidly along the boundary. While $\{v_\perp^2\}$ initially increase because random impulses accelerate ants, it later decreases because the fastest ants leave the arena interior first, reducing the average velocity among those that remain. In contrast $\{v_\parallel^2\}$, large initially, decreases monotonically because of the latter effect.

The velocities $\{v_\parallel^2\}$ and $\{v_\perp^2\}$ are expressed in units of v_∞ in Figure 4.3B. We have a rough estimate of $v_\infty = 5.3$ cm/s from the middle of shoulder feature in Figure 3.1. Using this and $\sigma_x^2 = 0.75$ (cm/s)^2, we have a basic time scale $\tau = 2.4$ s and length scale $\tau v_\infty = 12.8$ cm for the model. The size of the arena L
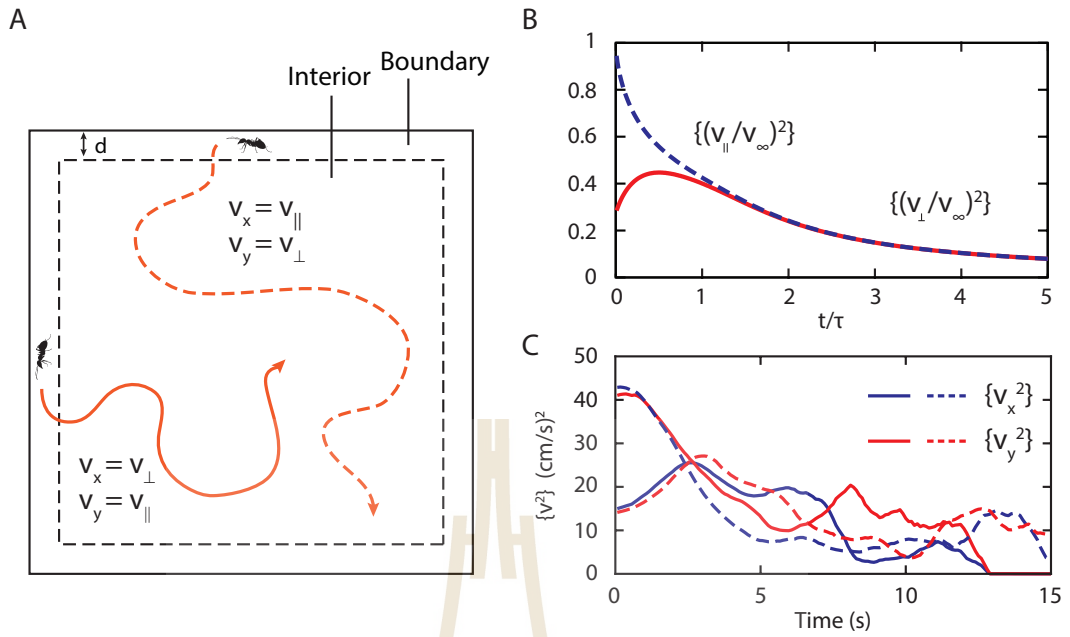
Figure 4.3 (A) Schematic of t-dependent of $\{v_\parallel^2\}$ and $\{v_\perp^2\}$ for ant entered an arena interior. The solid line (dashed line) depicts ants that ants entered an interior near arena boundary at $x = \pm L/2$ ($y = \pm L/2$) so the x-direction is perpendicular (parallel), and y-direction is parallel (perpendicular) to the boundary. **(B)** Model prediction: plot of $\{v_x^2\}$ (red solid curve) and $\{v_y^2\}$ (blue dashed curve) for ants in the arena interior versus time. Time is in units of τ, velocity is in units v_∞. **(C)** Experimental result of ants in a clean arena.

is comparable to $v_\infty \tau$, which means ants can come close to achieving equilibrium speed before exiting the arena interior.

The corresponding experimental quantity is also shown in Figure 4.3C, with $\{v_x^2(t)\}$ and $\{v_y^2(t)\}$ plotted for ants entering the interior from all four boundary strips. The velocity components perpendicular to the boundary strip from they entered behave like the model prediction for $v_\perp$ while parallel components behave like $v_\parallel$.

Seeing that the qualitative features of the model and the data are similar, we attempt a quantitative comparison. From the initial measured value of $\{v_\parallel^2\}$,

we get $v_\infty \approx 6.5$ cm/s, which is larger than the value $v_\infty = 5.3$ cm/s obtained from the peak of the shoulder feature. The time of the peak in $\{v_\perp^2(t)\}$ occurs at time $t/\tau \approx 0.5$ in the model and closer to $t \approx \tau$ in the experiment. The model agrees with the data to within a factor of order unity in both cases.

4.1.3.2 Position dependence of squared velocity

The model position dependence of $\{v_x^2\}$ and $\{v_y^2\}$ is sketched in Figure 4.4A. These quantities approach v_∞^2 in the open arena but are depressed at the boundaries and border to zone $\mathcal{R}$. Notably, they approach the same equilibrium value within zone $\mathcal{R}$, in the repellent, as in clean regions. Once a model ant overcomes the potential and arrives in zone $\mathcal{R}$, it forgets about this experience and random impulses restore its speed to v_∞.

Experimentally, $\{v_x^2\}$ and $\{v_y^2\}$, shown in Figure 4.4, are qualitatively consistent with model predictions. For the clean arena $\{v_x^2\}$ is small near the boundaries then rises to a maximum and becomes weakly position-dependent near the middle of the arena. The maximum of $\sqrt{\{v_x^2\}} \approx 5.4$ cm/s gives another experimental estimate of v_∞ that is consistent with previous values. The x-dependence of $\{v_y^2\}$ is dominated by boundary effects: near $x = \pm L/2$ most ants are moving quickly along the boundaries and $\sqrt{\{v_y^2\}} \approx 4.8$ cm/s is close to v_∞. Near $x = 0$, a large fraction of ants move rapidly along $y = \pm L/2$ with a small v_y component, so $\{v_y^2\}$ is reduced.

The repellent causes disturbances in $\{v_x^2\}$ at the borders to zone $\mathcal{R}$ but has no noticeable effect on $\{v_y^2\}$. When $\ell = 2.5$ cm, we see a depression in $\{v_x^2\}$ in zone $\mathcal{R}$. The expected recovery within zone $\mathcal{R}$ is, perhaps, faintly seen as the small peak occurring right at $x = 0$. This recovery is more clearly seen when $\ell = 10$ cm, as $\{v_x^2\}$ has minima at the borders to zone $\mathcal{R}$ and increases to either side of it.
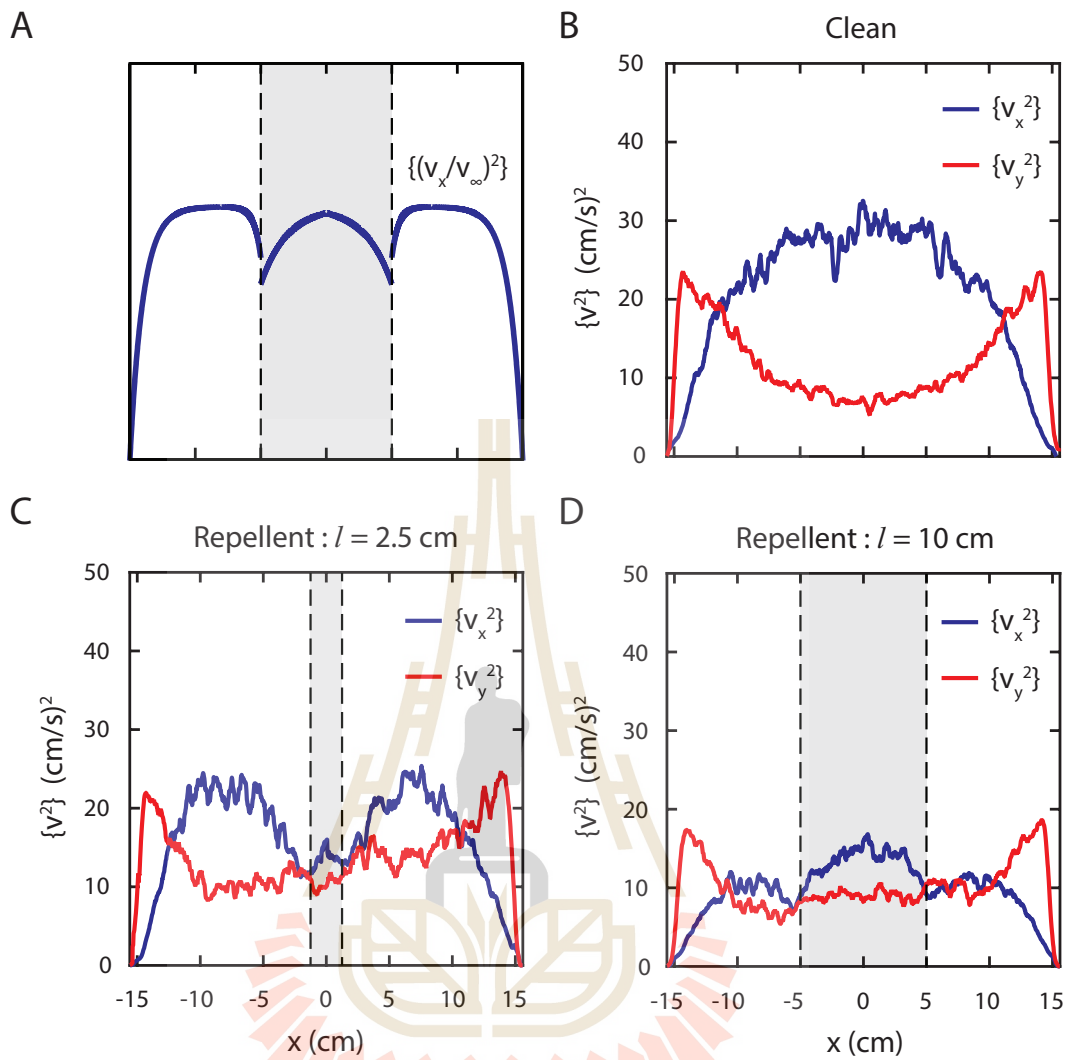
Figure 4.4 (A) Model prediction of x-dependent of $\{v_x^2\}$ and $\{v_y^2\}$ for ant entered an arena interior. The vertical scale is arbitrary. Experimental results, **(B)** plot for a clean arena. **(C)** The experiment where zone $\mathcal{R}$ was painted with $\ell = 2.5$ cm and **(D)** $\ell = 10$ cm.

We can see, from Figure 4.4, why shoulder features were missing from the distribution of v_x when repellent was present in zone $\mathcal{R}$, width $\ell = 10$ cm. Ants do not have enough space free from disturbances, between arena boundaries and the borders to zone $\mathcal{R}$, to achieve equilibrium velocity.

4.1.3.3 Field and potential

Supposing that the ant cannot leave the arena, the boundaries are associated with infinitely high potential barriers. For the repellent, we use a square potential barrier of height V_0. The associated field $E_x = -dV/dx$ is a pair of δ-function spikes, of opposite sign, at the borders to zone $\mathcal{R}$. These are depicted in Figure 4.5A. We gave the spikes finite width so they can be seen.

The experimental field $E_x = E_x(x)$ is obtained by ordering experimental data according to x and taking a running average over Δv_x. The corresponding potential is obtained by integrating this quantity. The results are shown in Figure 4.5. For the clean arena is shown in Figure 4.6C, the x-averaged value of Δv_x, interpreted as the field E_x, showed no position dependence within the arena. At the boundaries E_x is large over a short range, directed into the arena. These boundary fields, seen at $x = \pm L/2$ in Figure 4.5, look the same without or with repellent present.

With repellent in zone $\mathcal{R}$, we see spikes in the measured E_x at the borders to zone $\mathcal{R}$. The finite width of these spikes can be attributed to several factors. For one, the border to zone $\mathcal{R}$ is not well defined because the oil, even if perfectly painted, diffuses somewhat on the ceramic tile. For a more interesting one, the ant has finite spatial resolution in its determination of the field (i.e. its response to repellent) that varies according to the speed and angle at which it crosses into zone $\mathcal{R}$. The experimental potential $\{\Delta v_x\}$ is also plotted. A square barrier, roughly resembling the ideal model, is seen when the width of zone $\mathcal{R}$ is $\ell = 10$ cm. In the case of $\ell = 2.5$ cm, the square barrier has narrowed to a peak.

The experimental values for the height of the potential barrier V_0 fall in the range of $5 - 10$ (cm/s)^2. This value, much smaller than v_∞^2, is likely an underestimate of the potential barrier height. Determining the field and potential
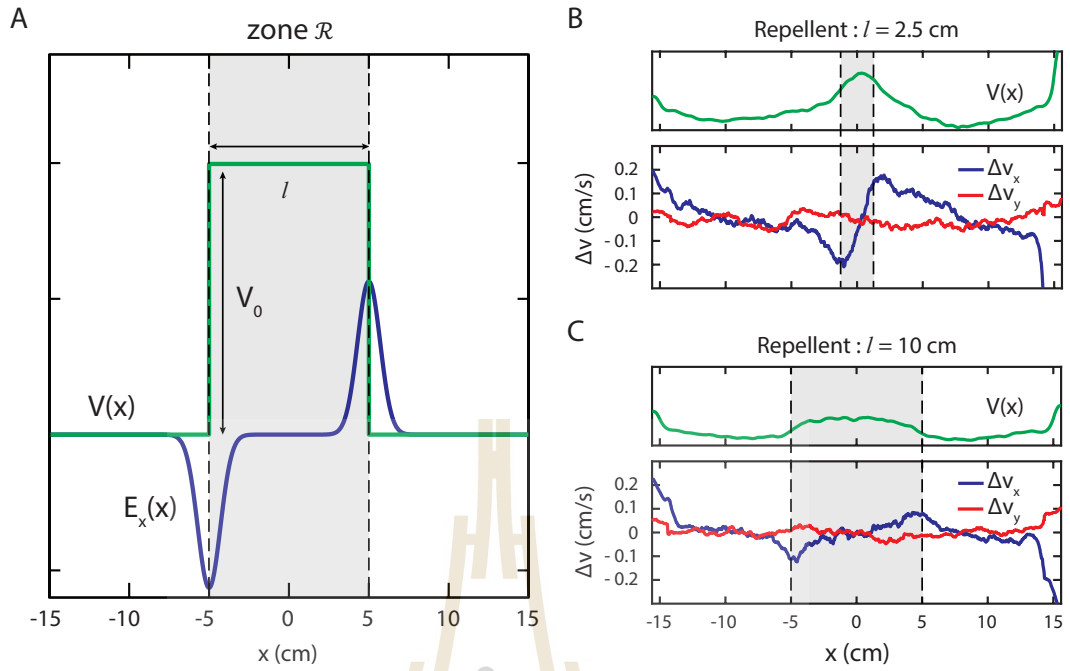
Figure 4.5 (A) Model prediction of the field and potential $V(x)$ versus position x, showing V_0 in zone $\mathcal{R}$. The vertical scale is arbitrary. Experimental results, running averages of Δv_x (blue) and Δv_y (red) versus position x with repellent when **(B)** $\ell = 2.5$ cm and **(C)** $\ell = 10$ cm.

in this manner is numerically delicate: one has to choose bins for the running-average that are big enough to ensure random impulses average to zero but small enough to preserve some spatial resolution.

Note that figure 4.6 plots of $\{\Delta v_x\}$ and $\{\Delta v_y\}$ versus time t, velocity v_x and position x for a clean arena. Recall that such plots are constructed by ordering the data set according to the time range of 3 s, a velocity range $\Delta v_x \approx 0.4$ cm/s, and a position range $\Delta x \leq 1$ cm. Then calculating a running average of each quantity (thus the curly brackets indicates an average over time and ants). The time-averages are small that is not apparent t-dependence, which as the expected result from symmetry. The velocity averages for Δv_x and Δv_y are also negligible, so that is not apparent v_x-dependence. While the running average of $\{\Delta v_x\}$ is
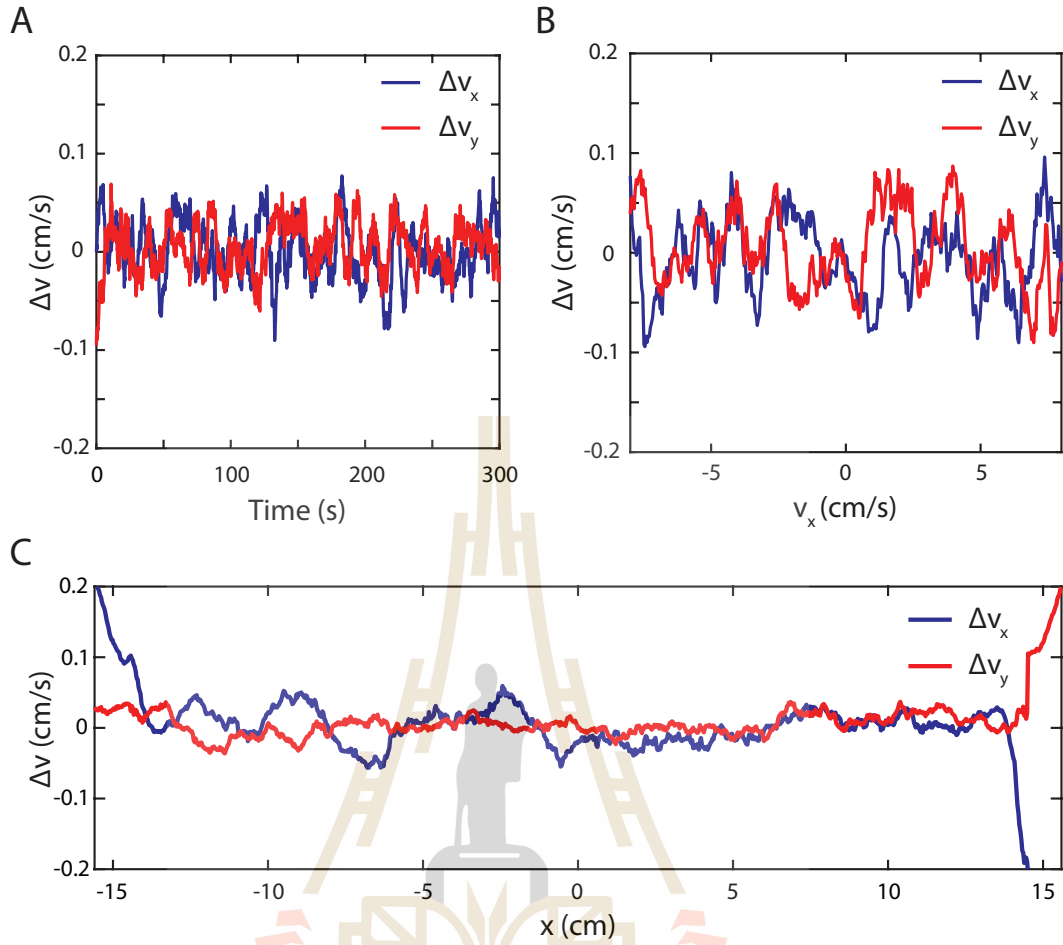
Figure 4.6 Running averages of Δv_x (black) and Δv_y (red) over time, velocity v_x, position x for all ants in a clean arena. **(A)** The running average of Δv over a 3 s time window ending at time t is small, with not apparent t-dependence. **(B)** The average of Δv between velocity $v_x - \Delta v_x$ and v_x where $\Delta v_x \approx 0.4$ cm/s is also small, with an apparent v_x-independence. **(C)** Position averages are approximately zero at all positions in a clean arena, excepted at the edges because of the boundary effect.

expected to give the field E_x due to the arena boundaries, it is found to be close to zero at all positions in the clean arena. The value $\{\Delta v_x\}$ should vanish due to symmetry and its measured value is indeed small.

4.1.3.4 Crossing probability and residence time

The crossing probability P_C and residence time T_R spent continuously in zone $\mathcal{R}$ were discussed above. According to model calculations, described in Section 3.4, P_C decreases with the size of the potential barrier V_0 because ants are slowed as they enter zone $\mathcal{R}$. So, P_C is always reduced by the effect of a repellent. The same slowing effect results in an initial increase in T_R with V_0, so a weak repellent will increase the time ants spend in zone $\mathcal{R}$ as compared to a clean region of the same size. With a sufficiently large V_0, T_R decreases because ants are immediately repelled.

Table 4.3 The measured probability P_C that an ant crosses zone $\mathcal{R}$, length ℓ, and measured time T_R it remains continuously in zone $\mathcal{R}$. Both depend on whether zone $\mathcal{R}$ has no repellent, i.e. is "Clean" or is coated evenly with the repellent citronella oil, "Repel".

		P_C	T_R (s)
$\ell = 10$ cm	Clean	0.91 ± 0.03	1.85 ± 0.08
	Repel	0.51 ± 0.04	2.08 ± 0.08
$\ell = 2.5$ cm	Clean	0.95 ± 0.02	0.52 ± 0.02
	Repel	0.79 ± 0.03	0.87 ± 0.04

We measured P_C and T_R the data subset in which the ant entered zone $\mathcal{R}$ with position $|y| < L/2 - d$, to reduce boundary effects and give the values in Table 4.3. For experiments in a clean arena, zone $\mathcal{R}$ has no physical meaning, but is merely the central strip $|x| < \ell$. The results are compared with experiments where the repellent, citronella oil, coated on zone $\mathcal{R}$. The crossing probability is lower when repellent is present. But ants reside within zone $\mathcal{R}$ for a longer time when it is infected with the chemical repellent than when clean. This counterintuitive

behavior agrees with the model prediction. It should be emphasized that the quantitative values of P_C and T_R calculated using our model, Section 3.4, do not agree with the data. For $\ell = 10$ cm and $\ell = 2.5$ cm, the model predictions of $P_C = 0.7$ and $P_C = 0.9$ are smaller than measured values. The residence times T_R, calculated using the crude but simplifying continuum approximation to the discrete random walk, were an order of magnitude smaller than measured values. But the qualitative effect of repellent on P_C and T_R is notable.

4.2 Summary

The simplistic theoretical model accounts for almost all statistical properties of ant motion in the experiment. Recall that the model includes a constant probability distribution function $p(\eta)$ for random impulses, with zero mean, mean-square σ^2 and negligible time correlations. It also includes a field due to interactions with the boundaries and the chemical repellent, where the latter can be adequately modelled by a scalar potential that has a positive value V_0 if repellent is present and is zero elsewhere. The navigation algorithm implied by this model is purely local, i.e. ants modify their path in response to their current position and velocity, without taking into account distant surroundings.

The theory is characterized by a small number of parameters: say v_∞, σ^2 and V_0, the first two of which are obtained form data for a clean arena. It provides a scheme for simulating motion in more general conditions.

CHAPTER V

CONCLUSION

The motion of individuals belonging to the species *Oecophylla smaragdina*, or weaver ants, was studied in a small arena by measuring the ant position as a function of time. The arena was a floor tile that was either clean or had a defined region coated with citronella oil, a substance that repels ants.

The aim of this thesis was to determine a simple model for the algorithm that governs ant navigation. It was originally intended to be the first stage in a larger project: a study of how communication between weaver ants affects their navigation. (Weaver ant communication is an active research area (Hölldobler and Wilson, 1978; Franks and Richardson, 2006; Gordon, 2010; Golden and Hill, 2016).) But we discovered along the way that the motion of an ant individual, alone in the arena with no companion to communicate with, has numerous interesting features. So, we decided to make this the sole subject of this thesis and relegated communication studies to future work.

We found that a version of Langevin theory of Brownian motion provides a good description of statistical properties of the data on individual ant motion. The equation of motion for ants is Newton's second law with a random force, with zero time-average and a fixed, robust probability distribution function $p(\eta) \sim exp\big(-|\eta|/(c_1\sigma)\big)$, where c_1 is a known constant of order unity, giving uncorrelated random impulses that act with each time step. The repellent can be modelled by an effective potential energy, and associated field, that results in ants receiving a negative impulse when they entire the region coated with repellent.

Most aspects of the data can be adequately accounted for with this minimal model, including counterintuitive properties such as the fact that ants spend more time continuously within a region with repellent present than they would in a clean region of the same size. The algorithm may be used to simulate motion, allowing investigations of more complex properties of motion to be done computationally.

The report above establishes a viable framework for studying weaver ant navigation. We now see that an ant individual moves according to Langevin theory and that its motion in a clean arena can be characterized by a single parameter σ. We know further that the ant responds to a mild chemical repellent in a manner analogous to the response of a Newtonian particle encountering a step potential: it suffers an impulse when it passes from a clean region to one infected by a repellent. The size of the impulse is given by the measurable parameter V_0, the height of the potential.

This work provides a good baseline for planned future studies of communication. In such studies, one can look for changes in σ and V_0 that occur after an ant individual has communicated with another. It will thus be possible to infer how ants direct the motion of their companions. Such studies can be done in a purely quantitative manner: effects of shared information will show up in the variation of parameters measured from statistical data. There is no need for any intrusion into the data analysis by researchers making subjective judgments and characterization. In our opinion, other animal-behavior researchers would benefit by following this objective methodology.

We hope to have contributed in a significant way to the study of weaver ant navigation and, in a small way, to the study of complex interacting systems.
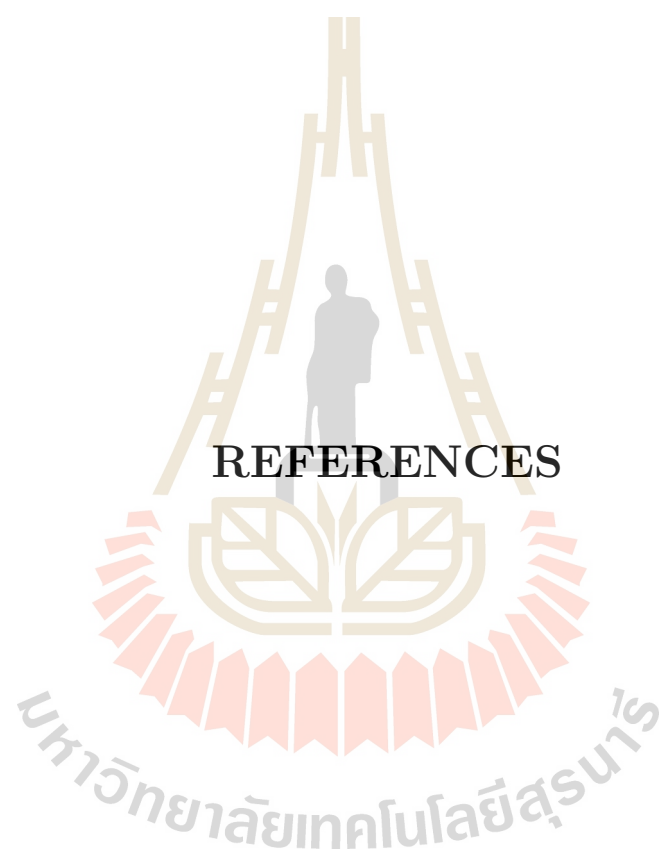
REFERENCES

REFERENCES

Altmann, J. (1974). Observational study of behavior: sampling methods. **Behaviour**, 49(3): 227–266.

Audira, G., Sampurna, B., Juniardi, S., Liang, S.-T., Lai, Y.-H., and Hsiao, C.-D. (2018). A simple setup to perform 3d locomotion tracking in zebrafish by using a single camera. **Inventions**, 3(1): 11.

Ballerini, M., Cabibbo, N., Candelier, R., Cavagna, A., Cisbani, E., Giardina, I., Lecomte, V., Orlandi, A., Parisi, G., Procaccini, A., Viale, M., and Zdravkovic, V. (2008). Interaction ruling animal collective behavior depends on topological rather than metric distance: Evidence from a field study. **Proceedings of the national academy of sciences**, 105(4): 1232–1237.

Bazazi, S., Bartumeus, F., Hale, J. J., and Couzin, I. D. (2012). Intermittent motion in desert locusts: behavioural complexity in simple environments. **PLoS computational biology**, 8(5): e1002498.

Becco, C., Vandewalle, N., Delcourt, J., and Poncin, P. (2006). Experimental evidences of a structural and dynamical transition in fish school. **Physica A: Statistical Mechanics and its Applications**, 367: 487–493.

Bialek, W. (2012). Biophysics: searching for principles. Princeton University Press.

Camargo, R. d. S., Puccini, C., Forti, L. C., and De Matos, C. A. O. (2017). Allogrooming, self-grooming, and touching behavior: contamination routes of leaf-cutting ant workers using a fat-soluble tracer dye. **Insects**, 8(2): 59.

Chung, Y.-K. and Lin, C.-C. (2017). Heat-induced symmetry breaking in ant (hymenoptera: Formicidae) escape behavior. **PloS one**, 12(3): e0173642.

Cole Jr, A. and Jones Jr, J. (1948). A study of the weaver ant, oecophylla smaragdina (fab.). **American Midland Naturalist**, 39(3): 641–651.

Czirók, A., Vicsek, M., and Vicsek, T. (1999). Collective motion of organisms in three dimensions. **Physica A: Statistical Mechanics and its Applications**, 264(1-2): 299–304.

Dankert, H., Wang, L., Hoopfer, E. D., Anderson, D. J., and Perona, P. (2009). Automated monitoring and analysis of social behavior in drosophila. **Nature methods**, 6(4): 297.

Deisboeck, T. S. and Couzin, I. D. (2009). Collective behavior in cancer cell populations. **Bioessays**, 31(2): 190–197.

DeLellis, P., Polverino, G., Ustuner, G., Abaid, N., Macrì, S., Bollt, E. M., and Porfiri, M. (2014). Collective behaviour across animal species. **Scientific reports**, 4: 3723.

Dell, A. I., Bender, J. A., Branson, K., Couzin, I. D., de Polavieja, G. G., Noldus, L. P., Pérez-Escudero, A., Perona, P., Straw, A. D., Wikelski, M., and Brose, U. (2014). Automated image-based tracking and its application in ecology. **Trends in ecology & evolution**, 29(7): 417–428.

Esponda, F. and Gordon, D. M. (2015). Distributed nestmate recognition in ants. **Proceedings of the Royal Society B: Biological Sciences**, 282(1806): 20142838.

Franks, N. R. and Richardson, T. (2006). Teaching in tandem-running ants. **Nature**, 439(7073): 153.

Gire, D. H., Kapoor, V., Arrighi-Allisan, A., Seminara, A., and Murthy, V. N. (2016). Mice develop efficient strategies for foraging and navigation using complex natural stimuli. **Current Biology**, 26(10): 1261–1273.

Golden, T. and Hill, P. (2016). The evolution of stridulatory communication in ants, revisited. **Insectes sociaux**, 63(2): 309–319.

Gordon, D. M. (2010). Ant encounters: interaction networks and colony behavior, volume 1. Princeton University Press.

Hölldobler, B. (1983). Territorial behavior in the green tree ant (oecophylla smaragdina). **Biotropica**, pages 241–250.

Hölldobler, B. and Wilson, E. O. (1978). The multiple recruitment systems of the african weaver ant oecophylla longinoda (latreille)(hymenoptera: Formicidae). **Behavioral Ecology and Sociobiology**, 3(1): 19–60.

Hölldobler, B. and Wilson, E. O. (1990). The ants. Harvard University Press.

Hölldobler, B. and Wilson, E. O. (1994). Journey to the ants: a story of scientific exploration. Belknap Press of Harvard University Press.

Humphries, N. E., Queiroz, N., Dyer, J. R. M., Pade, N. G., Musyl, M. K., Schaefer, K. M., Fuller, D. W., Brunnschweiler, J. M., Doyle, T. K., Houghton, J. D. R., Hays, G. C., Jones, C. S., Noble, L. R., Wearmouth, V. J., Southall, E. J., et al. (2010). Environmental context explains lévy and brownian movement patterns of marine predators. **Nature**, 465(7301): 1066.

Kamhi, J. F., Nunn, K., Robson, S. K., and Traniello, J. F. (2015). Polymorphism and division of labour in a socially complex ant: neuromodulation of aggression in the australian weaver ant, oecophylla smaragdina. **Proceedings of the Royal Society B: Biological Sciences**, 282(1811): 20150704.

Kohler, M. and Wehner, R. (2005). Idiosyncratic route-based memories in desert ants, melophorus bagoti: how do they interact with path-integration vectors? **Neurobiology of learning and memory**, 83(1): 1–12.

Krieger, M. J., Billeter, J.-B., and Keller, L. (2000). Ant-like task allocation and recruitment in cooperative robots. **Nature**, 406(6799): 992.

Kube, C. R. and Bonabeau, E. (2000). Cooperative transport by ants and robots. **Robotics and autonomous systems**, 30(1-2): 85–101.

Landau, L. D. and Lifshitz, E. (1980). Statistical physics, part 1: Volume 5.

Long, J., Zucker, S. W., and Emonet, T. (2017). Feedback between motion and sensation provides nonlinear boost in run-and-tumble navigation. **PLoS computational biology**, 13(3): e1005429.

Lukeman, R., Li, Y.-X., and Edelstein-Keshet, L. (2010). Inferring individual rules from collective behavior. **Proceedings of the National Academy of Sciences**, 107(28): 12576–12580.

Macnab, R. M. and Koshland, D. (1972). The gradient-sensing mechanism in bacterial chemotaxis. **Proceedings of the National Academy of Sciences**, 69(9): 2509–2512.

Mlot, N. J., Tovey, C. A., and Hu, D. L. (2011). Fire ants self-assemble into waterproof rafts to survive floods. **Proceedings of the National Academy of Sciences**, 108(19): 7669–7673.

Palavalli-Nettimi, R. and Narendra, A. (2018). Miniaturisation decreases visual navigational competence in ants. **Journal of Experimental Biology**, 221(7): jeb177238.

Pathria, R. and Beale, P. (1996). Statistical Mechanics. Elsevier.

Pokhrel, A. and Kayastha, P. (2018). Physics of collective animal behaviour: Making a leap from inanimate particles and atoms to conscious social animals. Retrieved May 6, 2019, from website https://xsigsummer.wordpress.com/2018/06/29/physics-of-collective-animal-behaviour-making-a-leap-from-inanimate-particles-and-atoms-to-conscious-social-animals/.

Raichlen, D. A., Wood, B. M., Gordon, A. D., Mabulla, A. Z., Marlowe, F. W., and Pontzer, H. (2014). Evidence of lévy walk foraging patterns in human hunter–gatherers. **Proceedings of the National Academy of Sciences**, 111(2): 728–733.

Reynolds, A. (2012). Distinguishing between lévy walks and strong alternative models. **Ecology**, 93(5): 1228–1233.

Reynolds, A. M. and Rhodes, C. J. (2009). The lévy flight paradigm: random search patterns and mechanisms. **Ecology**, 90(4): 877–887.

Romanczuk, P., Bär, M., Ebeling, W., Lindner, B., and Schimansky-Geier, L. (2012). Active brownian particles. **The European Physical Journal Special Topics**, 202(1): 1–162.

Sakiyama, T. (2017). Ant droplet dynamics evolve via individual decision-making. **Scientific reports**, 7(1): 14877.

Schultheiss, P., Cheng, K., and Reynolds, A. M. (2015). Searching behavior in social hymenoptera. **Learning and Motivation**, 50: 59–67.

Schweitzer, F., Ebeling, W., and Tilch, B. (1998). Complex motion of brownian particles with energy depots. **Physical Review Letters**, 80(23): 5044.

Shimizu, T. S., Tu, Y., and Berg, H. C. (2010). A modular gradient-sensing network for chemotaxis in escherichia coli revealed by responses to time-varying stimuli. **Molecular systems biology**, 6(1).

Sims, D. W., Humphries, N. E., Bradford, R. W., and Bruce, B. D. (2012). Lévy flight and brownian search patterns of a free-ranging predator reflect different prey field characteristics. **Journal of Animal Ecology**, 81(2): 432–442.

Sims, D. W., Southall, E. J., Humphries, N. E., Hays, G. C., Bradshaw, C. J., Pitchford, J. W., James, A., Ahmed, M. Z., Brierley, A. S., Hindell, M. A., Morritt, D., Musyl, M. K., Righton, D., Shepard, E. L. C., Wearmouth, V. J., et al. (2008). Scaling laws of marine predator search behaviour. **Nature**, 451(7182): 1098.

Szurmant, H. and Ordal, G. W. (2004). Diversity in chemotaxis mechanisms among the bacteria and archaea. **Microbiol. Mol. Biol. Rev.**, 68(2): 301–319.

Tinbergen, N. (1963). On aims and methods of ethology. **Ethology**, 20(4): 410–433.

Tong, D. (2012). Lectures note on Statistical Physics. University of Cambridge.

Vernerey, F. J., Shen, T., Sridhar, S. L., and Wagner, R. J. (2018). How do fire ants control the rheology of their aggregations? a statistical mechanics approach. **Journal of The Royal Society Interface**, 15(147): 20180642.

Vicsek, T., Czirók, A., Ben-Jacob, E., Cohen, I., and Shochet, O. (1995). Novel type of phase transition in a system of self-driven particles. **Physical review letters**, 75(6): 1226.

Vicsek, T., Czirók, A., Farkas, I. J., and Helbing, D. (1999). Application of

statistical mechanics to collective motion in biology. **Physica A: Statistical Mechanics and its Applications**, 274(1-2): 182–189.

Vicsek, T. and Zafeiris, A. (2012). Collective motion. **Physics reports**, 517(3-4): 71–140.

Viswanathan, G. M., Buldyrev, S. V., Havlin, S., Da Luz, M., Raposo, E., and Stanley, H. E. (1999). Optimizing the success of random searches. **nature**, 401(6756): 911.

Wang, S., Cao, S., Wang, Q., Lian, L., and Song, W. (2016). Effect of exit locations on ants escaping a two-exit room stressed with repellent. **Physica A: Statistical Mechanics and its Applications**, 457: 239–254.

Wang, S., Lv, W., and Song, W. (2015). Behavior of ants escaping from a single-exit room. **PloS one**, 10(6): e0131784.

Wehner, R. (2003). Desert ant navigation: how miniature brains solve complex tasks. **Journal of Comparative Physiology A**, 189(8): 579–588.

West, B. J. and Nonnenmacher, T. (2001). An ant in a gurge. **Physics Letters A**, 278(5): 255–259.
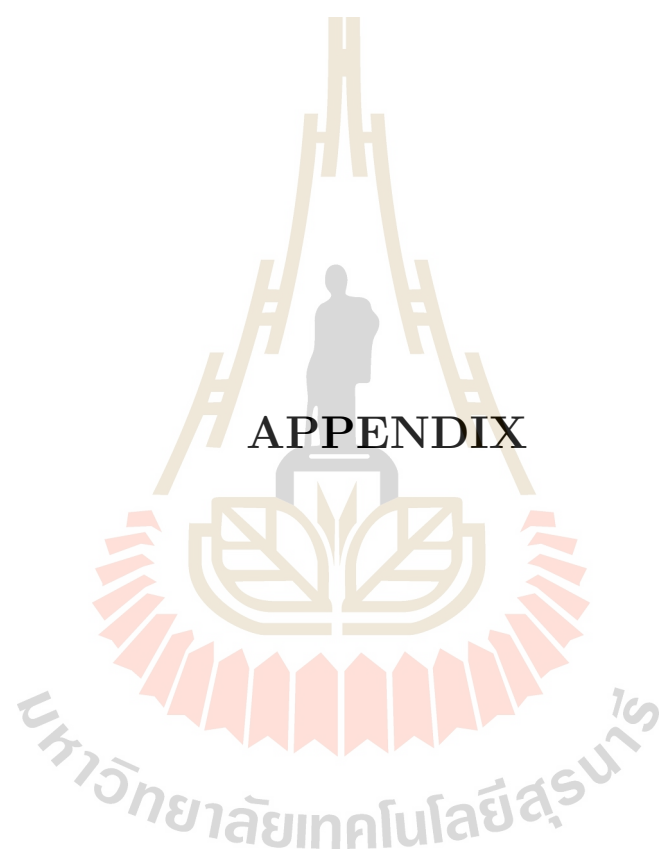
APPENDIX

APPENDIX A

CHI-SQUARED TEST

To fit the probability distribution of velocity changes $p(\Delta v_x)$ and $p(\Delta v_y)$, we initially used both parameters σ and m appearing in Eq.3.2. For given values of σ and m, the values of $\chi^2 = \chi^2(\sigma, m)$, the average squared difference between the data and Eq.3.2, was calculated. In Figure A.1, we show χ^2 over a range $0 < \sigma < 3$ and $0 < m < 2$ for the case where $|x| < L/2 - d, |y| < L/2 - d$ in a clean arena (this is a subset free from boundary effect). The blue-dot in the figure indicates the point σ, m where χ^2 is minimum.

There is a valley in Figure A.1, surrounding the minimum, in which χ^2 remains fairly close to its minimum value. We take advantage of this by fixing $m = 1$ and finding the σ that minimized χ^2. That is, we approximated the best two-parameter fit by the best one-parameter fit with $m = 1$. A Gaussian, $\sigma = 2$ lies outside this valley and, moreover, Gaussian fits do not have the appropriate qualitative shape near the origin.
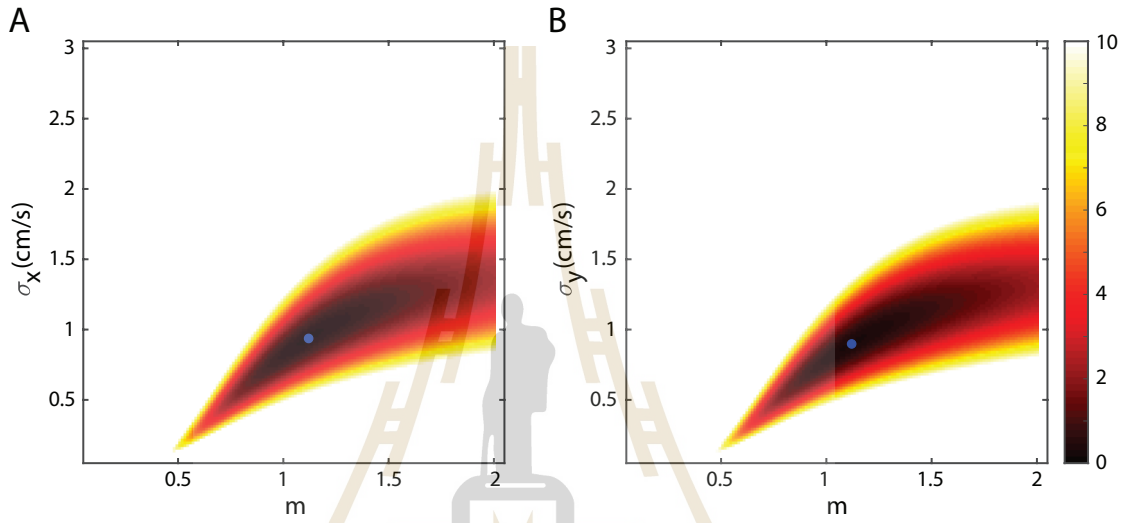
Figure A.1 The χ^2 value, obtained from fits of the experimental histograms of (A) $p(\Delta v_x)$ and (B) $p(\Delta v_y)$ to Eq.3.2, is color-plotted as a function of the two free parameters m and σ of Eq.3.2. Darker color indicates a smaller value of χ^2 and thus a better fit. The optimal values (A) $m = 1.12$ and $\sigma_x = 0.94$ (cm/s), (B) $m = 1.12$ and $\sigma_y = 0.90$ (cm/s), are indicated by the small blue dots. Since χ^2 remains comparably small over a broad region in (m, σ), it is convenient to fix $m = 1$ and then use σ as the only fitting parameter.

CURRICULUM VITAE

NAME: Theerawee Thiwatwaranikul   **GENDER**: Male

NATIONALITY: Thai   **DATE OF BIRTH**: March 31, 1994

EDUCATIONS:

- July 2016, Bachelor Degree of Science in Physics, Honors Program (First Class Honors), Suranaree University of Technology, Nakhon Ratchasima, Thailand

- March 2011, Finished Senior High School (Grade 12), Surawittayakarn School, Surin, Thailand

- March 2005, Finished Junior High School (Grade 9), Anubarnsurin School, Surin, Thailand

PUBLICATIONS:

-

GRANTS AND FELLOWSHIPS:

- Received the scholarship of Kittibundit Scholarship, Suranaree University of Technology, since 2016-2017